

We began our joint project with a kickoff meeting in Woods Hole in September 2008. During that meeting, our overall objectives were refined and initial milestones were identified. The major activities thus identified were the following:

- The consolidation and synthesis of *C. finmarchicus* data for the North Atlantic;
- The implementation and validation of a low-resolution workbench (LRW) model for the combined North Atlantic / Arctic Ocean system, inclusive of sea ice dynamics and ecosystems; application of this model to produce a 50-year retrospective simulation of the coupled physical/biological state in the North Atlantic;
- The design and testing of a high-resolution workbench (HRW) model; application to a multi-year hindcast in the North Atlantic to assess the contributions of (e.g.) mesoscale processes;
- The addition of the COSiNE ecosystem model to ROMS; evaluation and interpretation of the resulting coupled model in both the LRW and HRW configurations;
- The design of the inversion methodology to be used (ROMS + *Calanus* model); conduct of inversions for the “mean state” of *C. finmarchicus* populations in the North Atlantic and interpretation of results;
- The use of *Calanus* genetic data to estimate the rate of population exchange among the North Atlantic gyres; and
- The investigation of inter-annual to decadal scale variability in (e.g.) inter-gyre connectivity in both the past and (predicted) future North Atlantic.

The combined project team has continued to make sustained progress across these science and technical areas, as follows.

### ***C. finmarchicus* data (WHOI)**

Previously, we had obtained the mean monthly *C. finmarchicus* data from Grégory Beaugrand, and mapped these observations onto a grid suitable for model initialization. The distributions are similar to those reported by Planque et al. (1997), indicating the updated data set has essentially the same characteristics as this earlier assessment of *C. finmarchicus* climatology.

In the last year, we have also begun the task of assembling other published data sets for the North Atlantic *C. finmarchicus*. This work is being done in collaboration with the Jeff Runge and James Pierson project [Collaborative Research: Life histories of species in the genus *Calanus* in the North Atlantic and North Pacific Oceans and responses to climate forcing]. The data sets are being assembled and analyzed in order to provide data for setting boundary conditions and for comparisons to model hindcasts. There are a number of existing data sets, many resulting from the International GLOBEC programs in the North Atlantic. Of these, we have in hand, or are about to receive, data at the stations depicted in Figure 1. Features that are being assembled for *C. finmarchicus* are the distribution and abundance, rates of growth, reproduction, and mortality, and

overwintering depth and duration. We are also endeavoring to recover other historical data sets that are in papers and reports.

### Sites where data are in hand or about to be.

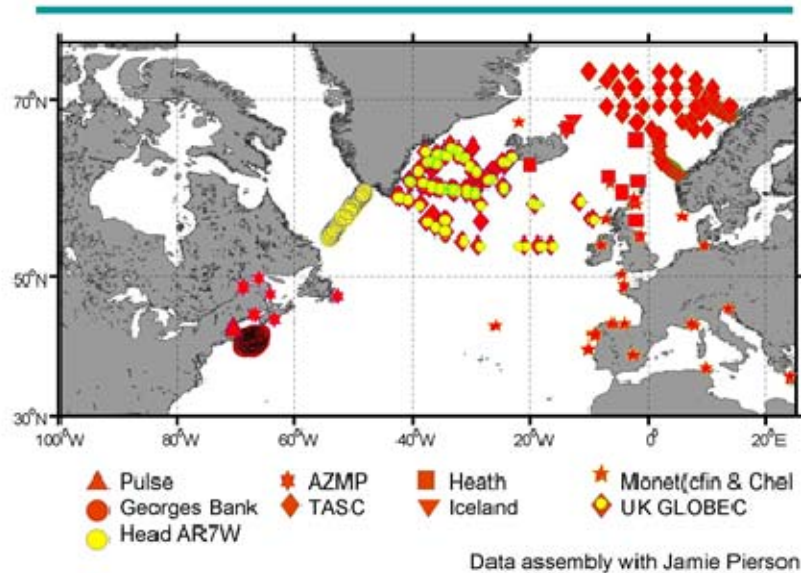


**Figure 1:** *C. finmarchicus* data sets being assembled.

### **High-resolution workbench (HRW) model (UMass-D & Rutgers) & Evaluation of the ROMS/COSiNE coupled model at high resolution (UMaine & UMass-D)**

In the first combined project meeting at WHOI in September 2008, it was decided that two parallel development tracks for the basin-scale modeling would be needed to achieve accelerated progress on both the bio-physical coupling and adjoint modeling studies. In addition to the low-resolution studies described further below, the project team at UMass-D has been pursuing a parallel implementation of the North Atlantic / Arctic model at higher ( $1/12^\circ$ ) resolution. A specific technical objective of this high-resolution workbench (HRW) effort is to achieve an accurate replication of the hydrologic cycle in the North Atlantic / Arctic system using a model with little (or no) salinity restoration.

Our research specifically addresses several mechanisms by which freshwater influx (or the lack thereof) might impact the population dynamics and production of *Calanus finmarchicus* in the North Atlantic. To address these objectives, we are (i) simulating basin-scale circulation fields from 1985-2007 using an eddy-resolving, validated model

extended to include sea ice and riverine inputs of fresh water; (ii) utilizing a 10-component (lower trophic level) biogeochemical model to understand the biophysical pathways connecting the three *Calanus* gyres during the GLOBEC decade from 1990 to 1999; and (iii) forecasting the next 20 years (*i.e.*, 2008-2028) of the state of the North Atlantic Ocean using idealized forcing fields (wind curl, heat flux, E-P) representing IPCC scenarios of climate change.

At UMass-D, the focus for the first year had been on setting up the high-resolution North Atlantic basin-scale model and the development of a salinity data base for validation. During the second year, the physical model was run successfully and the joint team of UMass-UMaine coupled the 10-component CoSiNE sub-model within the ROMS high-resolution workbench (HRW) model. During the second and third years, the high-resolution physical model was run in both physical and bio-physically-coupled mode at the NCAR supercomputing facility. Six years of physical simulation (1985-1991) and three years of a coupled biophysical run (1985, 1986, and 1989) are now complete. Analysis of these runs shows encouraging results for the seasonal variability of the temperature, currents and nutrient/silicate fields. However, there was a noticeable increasing trend in salinity in the upper 200-1500 meters of the water column, dominated by drifts in the polar and sub-polar regions. Similar results are also obtained in the Western North Atlantic, where (however) simulated salinity increases agree with RIVSUM trends during 1985-1990, the understanding of which will require further sub-regional analysis.

Diagnostic investigation led us to conclude that the drifts in simulated salinities might be reduced by: (i) reconsidering the initial ice field; (ii) opening the Bering Strait, until then closed; (iii) inclusion of a Mediterranean outflow condition; (iv) better parameterization of vertical mixing (KPP as opposed to GLS); (v) inclusion of inter-annual variability of rivers; and/or (vi) slow restoration of surface salinity. In the final year of this project, we will implement these changes and complete the physical, biophysical and climate simulations. We have already begun implementing the first three improvements and expect to complete the others by mid-summer, 2011. In this effort, we are guided, in part, by the results from the LRW studies ongoing at Rutgers (see below).

In the following, we describe the findings of the third year in segments of: (1) Physical model issues and future implementation plan, (2) Biogeochemical results and implementation plan, (3) Climate implementation plan, and (4) Summary of future tasks.

### *1. Physical model issues and future implementation plan*

The model grid is four times finer than the LRW, with higher resolution on the order of 5 km in the North Atlantic and Arctic, and lower resolution on the order of 50 km in the Equatorial and South Atlantic. There are 50 vertical levels in the model. The total grid size is 1258 x 780 x 50. The boundary conditions are derived from Simple Ocean Data Assimilation (SODA) reanalysis data [Carton et al., 2000 a, b], and atmospheric forcing is obtained from the Common Ocean-Ice Reference Experiment (CORE) data [Large and Yeager, 2004].

During the first year of this project, we started the physical simulation from 1985 as planned. However, the model simulations (with no salinity or temperature restoration) were drifting away from climatological/observational salinity ranges rather quickly. This is the first simulation (1985-1989) in year 1. After considerable debugging, it was realized that the run-off inputs were not properly synchronized in space and time during the model simulation. Once the run-off was synchronized, a second simulation was carried out (1985-1991) during the second year. This simulation had very robust physical circulation and temperature evolution (without restoring). Some of the results were described in the last annual report (2009-2010). Nonetheless, during this later simulation, a number of persistent salinity drifts were noticeable, which are region-specific (*e.g.*, salting in Arctic shelves, salting in sub-polar regions, but freshening in the sub-tropics to tropics). We thus decided to diagnose this behavior first, before continuing to run long-term physical simulations. We return to the issue of potential model improvements below.

The physical circulation model at high resolution has been validated against annual climatological T-S profiles and circulation fields. The model skill for its 5-year average is compared against the World Ocean Atlas (WOA; 2005) data in Figure 2 in a Taylor diagram (Taylor, 2001). The Taylor diagram provides a statistical summary of how well model simulation and observation patterns match each other in terms of their correlation coefficient, their root-mean-square difference, and the ratio of their standard deviations. The radial distances from the origin and azimuthal positions in a typical Taylor Diagram (Figure 2) represent the standard deviations and correlation coefficients respectively, which measure model-observation differences in phase. The distances between the observation and simulations in Figure 2 represent model-observation root-mean-square errors which measure differences in amplitude. Simulation features that match well with observations in both amplitude and phase appear closest to the observed point (marked OBS) in the diagram. The model climatology parameters (SST, SSS, Ice concentration, mixed layer depth, Nitrate, Silicate) were determined by computing 1-degree bin averages from 5-years of simulation.

Despite the general agreement suggested in the Taylor diagram, the simulated hydrological cycle was found to be deviating from the climatology which prompted us to investigate the salinity simulation further. It was found that the mean model salinity was slowly increasing over the whole domain at 0.20 psu per year. The volume-averaged salinity drift is shown in Figure 3.

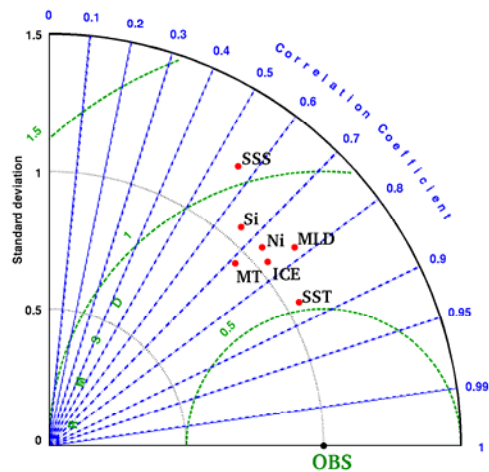


**Figure 2.** Taylor diagram presentation of the HRW model climatology compared against WOA climatology.

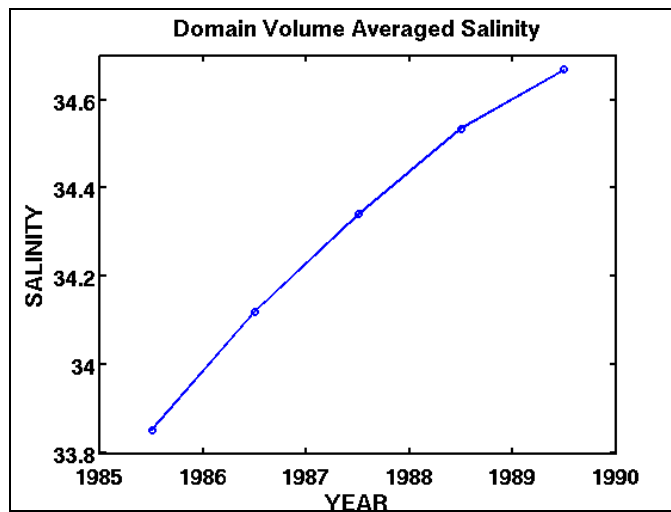


**Figure 3.** Volume-averaged salinity drift from the five years of simulation.

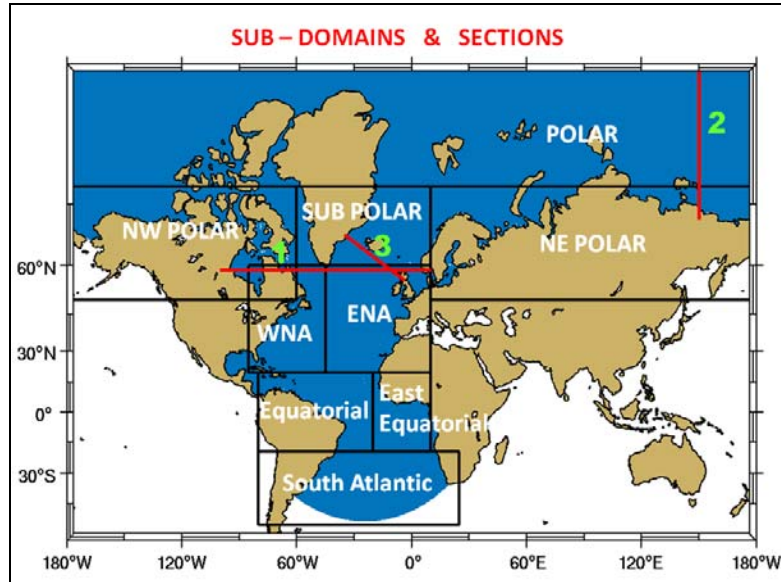
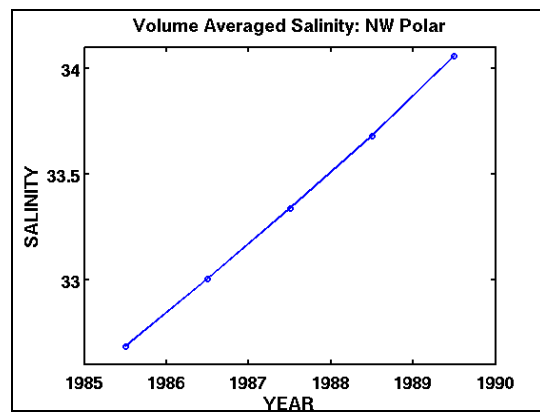
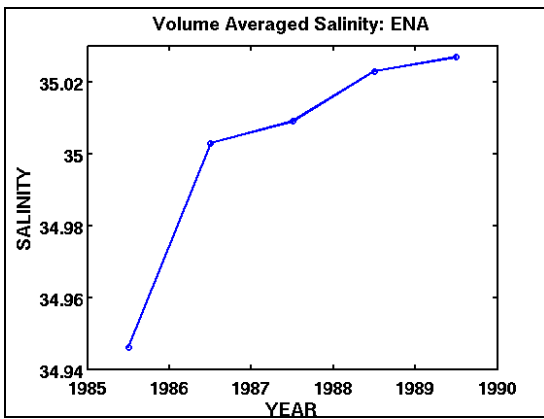
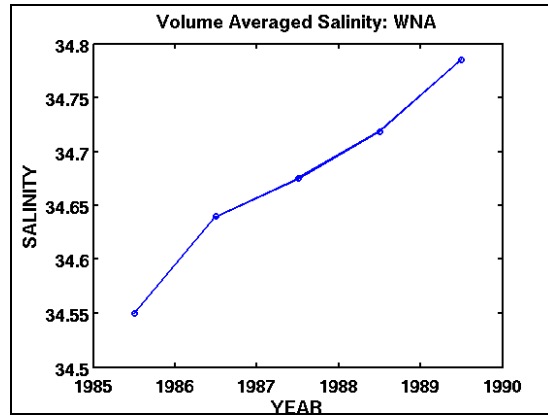
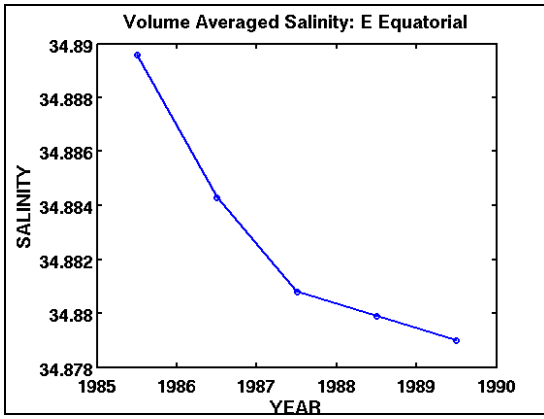
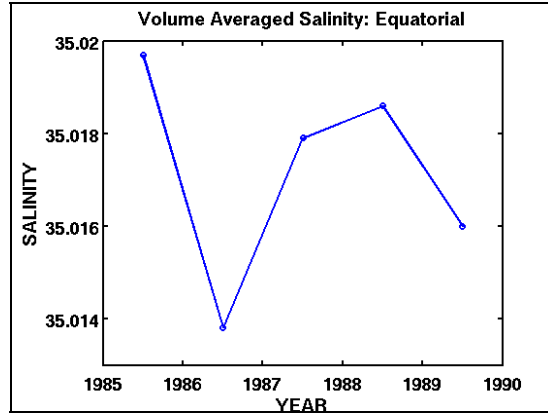
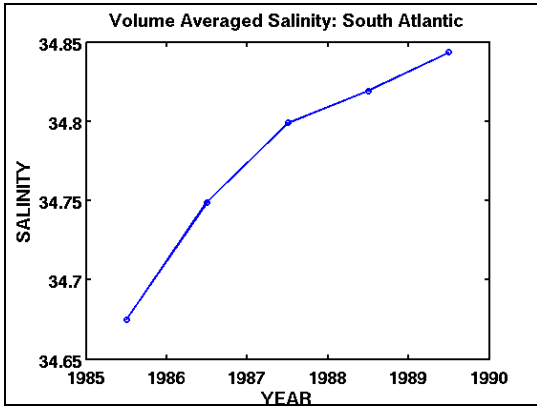


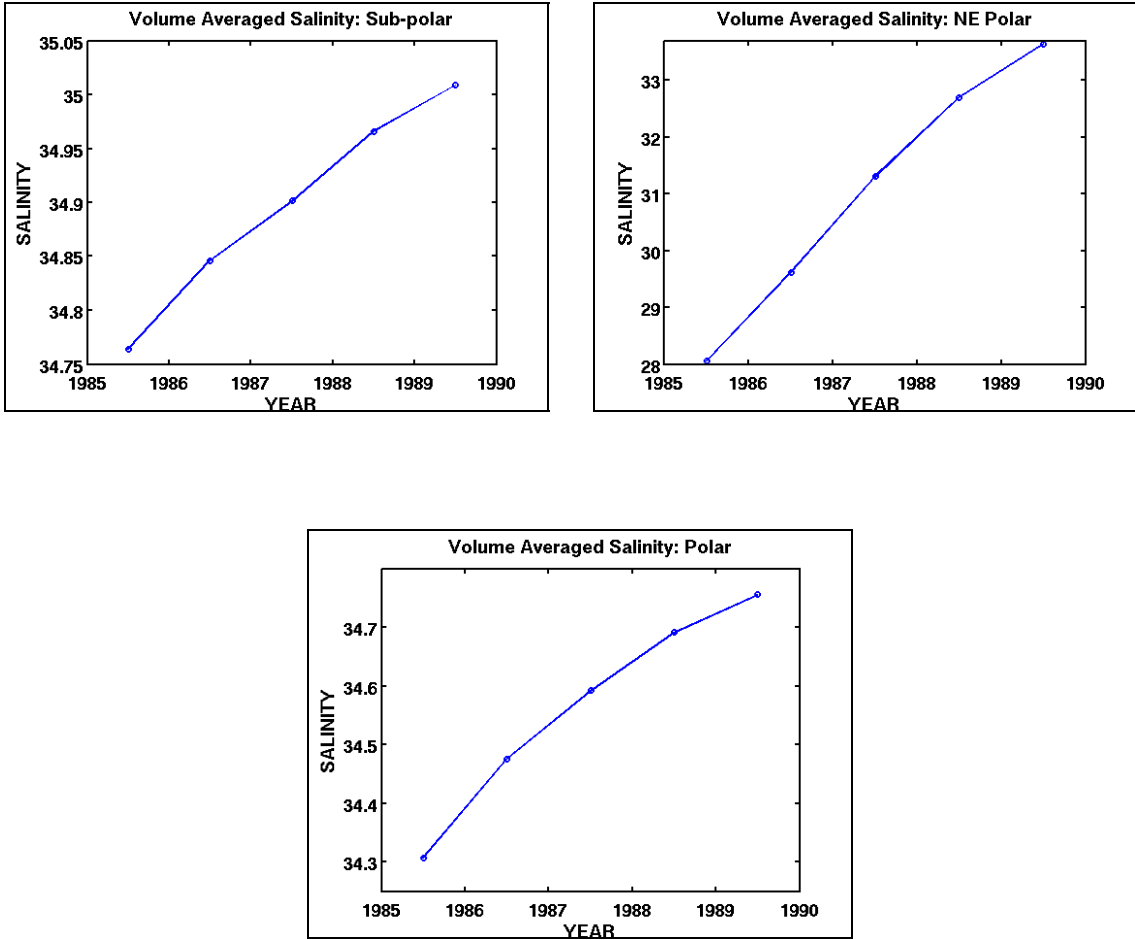
**Figure 4.** Sub-domains and sections (1, 2 and 3) for investigating the hydrological cycle.

To understand the spatial distribution of this drift, we sub-divided the whole domain into nine sub-domains (Figure 4). Volume-averaged salinity is then computed for each of the nine sub-domains for each of the five years. Figure 5 shows the salinity drift for these sub-domains, and Table 1 lists the numbers for the corresponding volume-averaged salinity. From Table 1 and Figure 5 it is evident that the change in salinity in the South Atlantic, Equatorial, East Equatorial and ENA is small compared to that within the WNA, NW Polar, Sub-Polar, NE Polar and Polar Regions.

The depth-wise salinity change has also been examined to determine the drift of salinity with depth (0 - 100 m, 100 - 200 m, 200 - 500 m, 500 - 1000 m, 1000 - 2000 m, 2000 - 4000 m and 4000 - 6000 m). This depth-dependence of the drift for the nine sub-domains is shown in Figure 6.

For the South Atlantic, Equatorial and Eastern Equatorial sub-domains, the averaged salinity for the five years first decreases up to 1000 m, and then the salinity increases, and finally becomes constant around 2000 m deep. The rest of the six sub-domains have a different trend. In the WNA region, the salinity decreases in the upper 1000 m, after which the drift is reversed with an overall impact of increasing trend over the five years. In the NW Polar region, the salinity drift increases to 1000m, and then the drift becomes negligible. In the Sub-Polar Region the salinity drift first increases to 1000 m and then it decreases. For the NE Polar region the salinity drift is very distinct in the upper 200 m, and it remains constant below 1000 m. In the Polar Region the drift is also in the upper 1000 m of the ocean, and remains the same at depth below 2000 m. It is clear that in all the 9 sub-domains the drift takes place in the upper 1000 - 1500 m of the ocean.

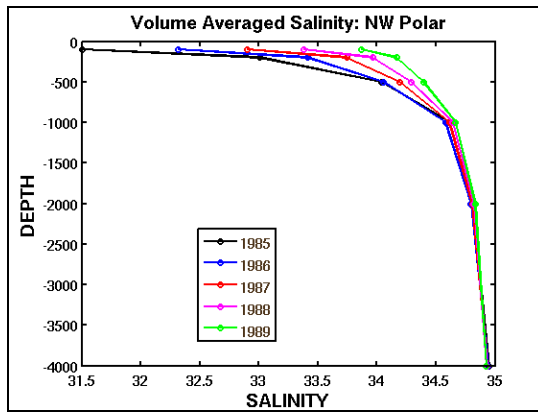
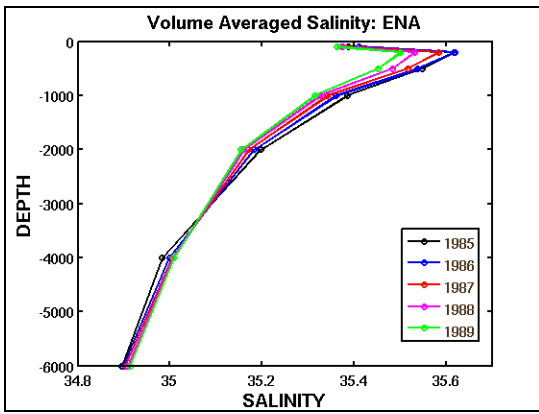
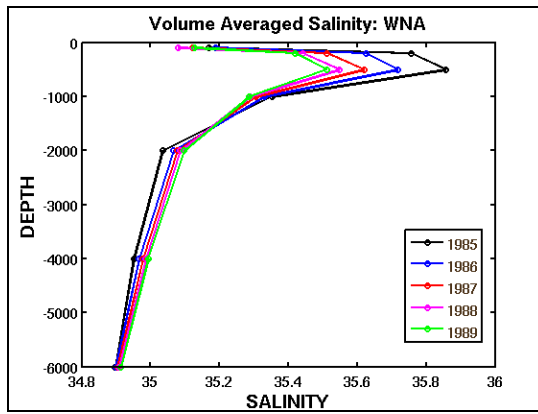
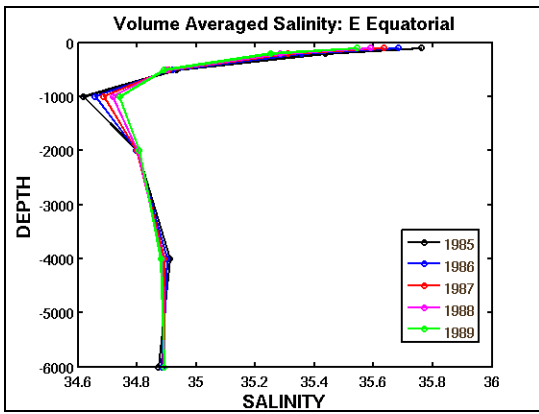
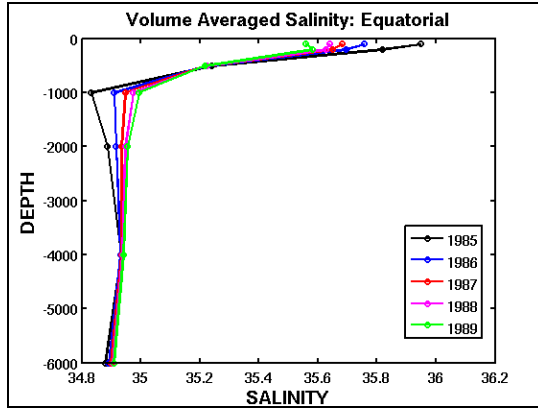
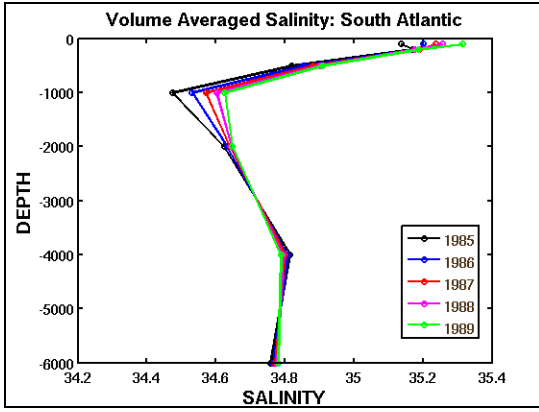




**Figure 5.** Volume-averaged salinity drifts for the 9 sub-domains.

**Table 1.** Region-wise salinity drifts.

	<b>1985</b>	<b>1986</b>	<b>1987</b>	<b>1988</b>	<b>1989</b>	<b>Drift (psu/year)</b>
<b>South Atlantic</b>	34.6747	34.7488	34.7991	34.8193	34.8434	0.0422
<b>Equatorial</b>	35.0197	35.0138	35.0179	35.0186	35.0160	-0.0009
<b>E_Equatorial</b>	34.8896	34.8843	34.8808	34.8799	34.8790	-0.0027
<b>WNA</b>	34.5500	34.6399	34.6749	34.7188	34.7852	0.0588
<b>ENA</b>	34.9462	35.0029	35.0090	35.0229	35.0268	0.0202
<b>NW_Polar</b>	32.6846	33.0035	33.3384	33.6806	34.0578	0.3433
<b>Sub_Polar</b>	34.7640	34.8461	34.9014	34.9659	35.0090	0.0612
<b>NE_Polar</b>	28.0569	29.6220	31.3091	32.7014	33.6437	1.3967
<b>Polar</b>	34.3070	34.4754	34.5920	34.6912	34.7555	0.1121
<b>Whole_Domain</b>	33.8528	34.1200	34.3406	34.5347	34.6676	0.2037



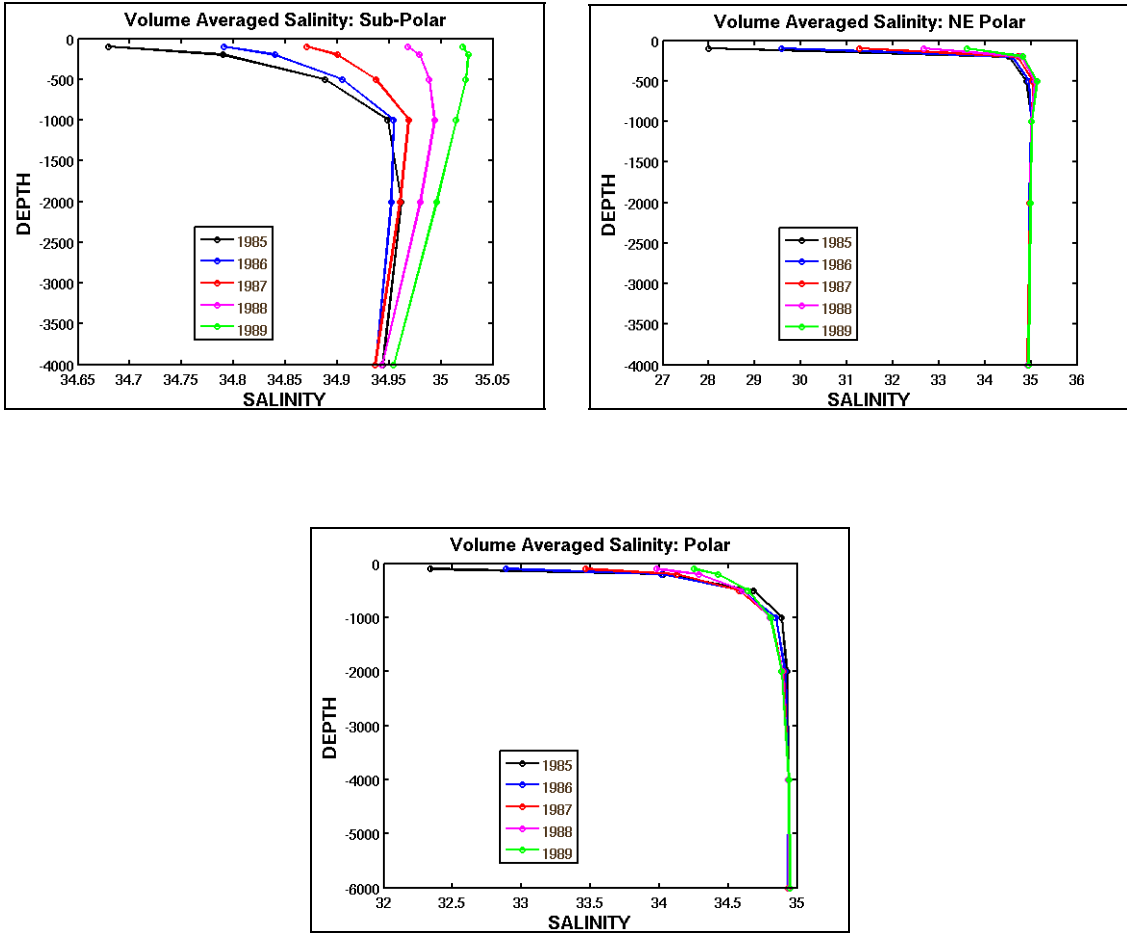


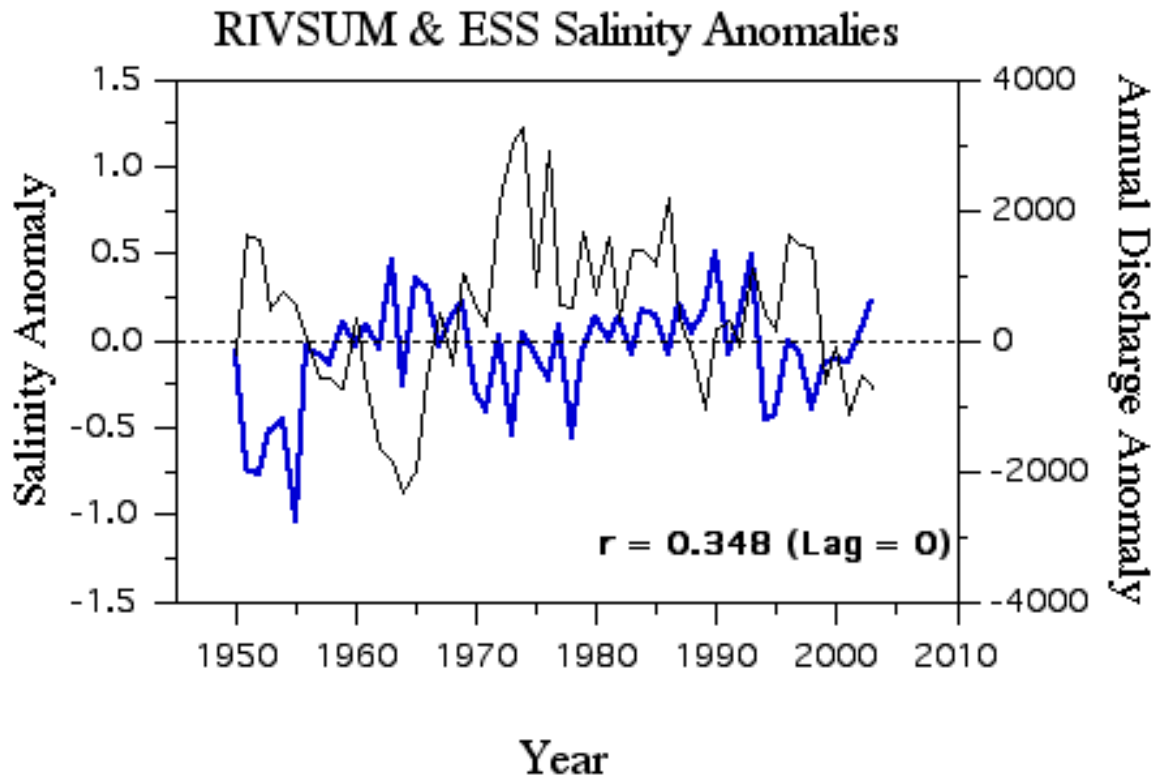
Figure 6. Depth-binned salinity of the sub-domains.

Discharge data (RIVSUM) from the Gulf of St. Lawrence shows decreasing values (Figure 7) over the 1985-1989 period while the Eastern Scotian Shelf (ESS) salinities increased (blue line in Fig. 7) in agreement with results for the simulated WNA (Fig. 5). Is this simply coincidence given the much larger region for the model WNA or actual agreement? The result in Figure 5 is based on the whole WNA region, which has many shelf regions and these behave differently than the slope and the Gulf Stream and Sargasso region. A detailed analysis over reduced-size regions to address the question whether or not the model salinity output reflects reality in some regions (away from the polar region) might be warranted.

To further understand the spatial structure of the salinity drift, a number of sections were studied (Figure 4). We present the result from only one section (Section 1, across 59N) next (Figure 8). A distinct and clear front can be seen in the shelf-slope area in both winter and summer, for both salinity and temperature. During winter, stratification is seen in between 200 – 400 m in 1985, which deepens to 400 – 600 m in 1986, and finally the stratified layer cannot be seen during 1987 – 1989. During summer 1985 the stratified layer is observed in between 200 – 600 m, which deepens to 400 – 1000 m in 1986 and by the end of 1989 no stratification is seen. So the sea water is becoming more salty in the upper 1000 m over the five years.

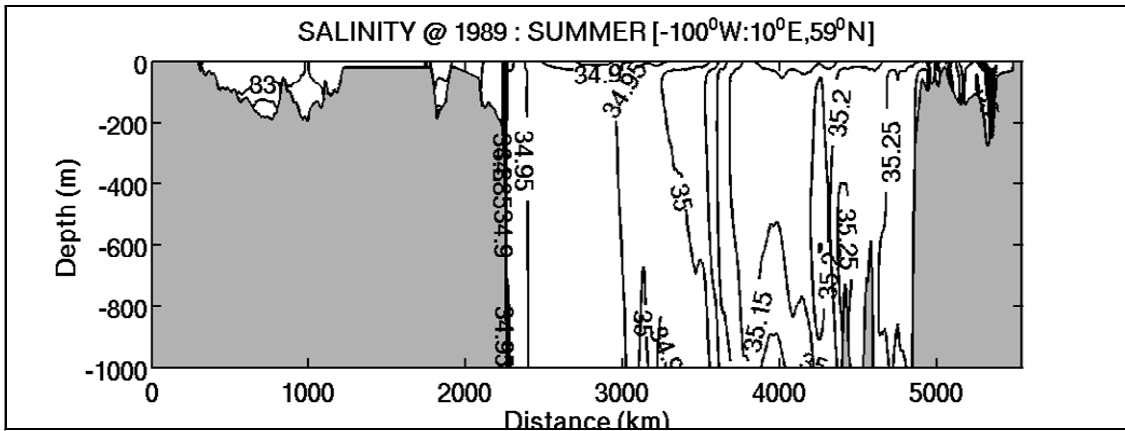
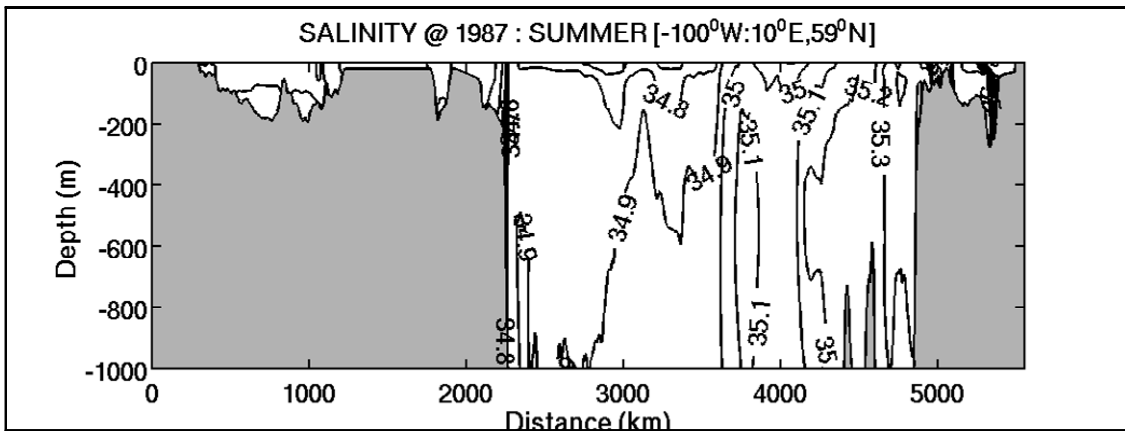
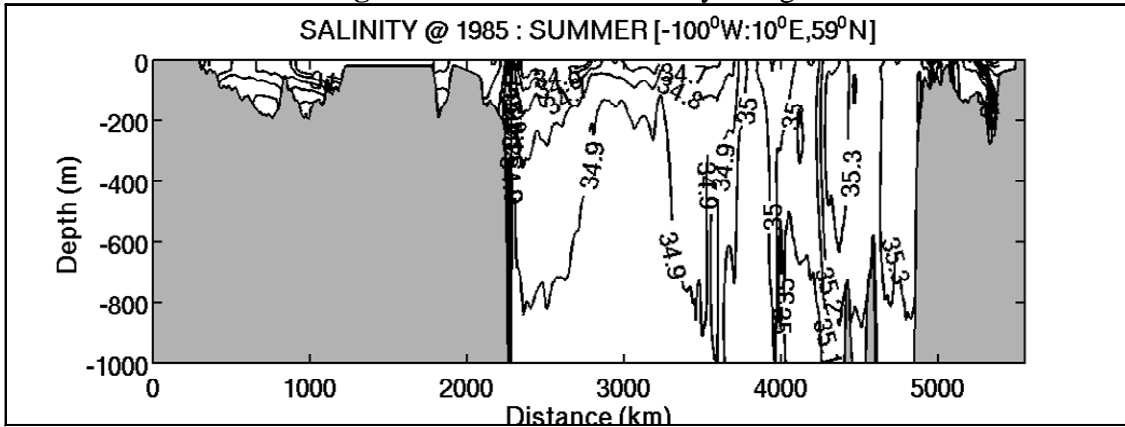
Lastly, the drift of sea ice volume over the five years has been computed to correlate it with the salinity drift. The sea ice volume for the sub-domains in WNA, NW Polar, Sub-Polar, NE Polar and Polar Regions, where the salinity drift is more apparent are shown in Figure 8. The seasonal formation and melt of sea ice is the dominant factor controlling the salinity and density of surface ocean waters in the Polar Regions. As the ocean water freezes to form sea ice, salt is expelled and thus the salinity of the ocean increases. The NE Polar, NW Polar and Polar Regions have the maximum volume of ice which may be responsible for the salinity drift. Note that these are the sub-regions with maximum drifts (Table 1). With the formation of more sea-ice over the years, the salinity increases, this is in accordance with the Figure 9. In NE Polar and Polar Regions there is a drop in the ice volume in 1988, and then it increases in 1989. But in the NW Polar Region the ice volume increases from 1985 to 1988, and then a sudden drop in ice volume in 1989.

The accumulation of sea ice over the course of the five-year simulation strongly implicates this as a factor in the anomalous increase in salinity in the upper water column in the ice-covered regions.



**Figure 7.** Annual discharge anomalies (RIVSUM) from the Gulf of St. Lawrence (black line) and the Eastern Scotian Shelf (ESS) salinity anomaly during 1950-2004. Note the increasing salinity trend on the ESS during 1985-1990. (from Bisagni, unpublished data)

**Figure 8:** Transects of salinity along section 1.



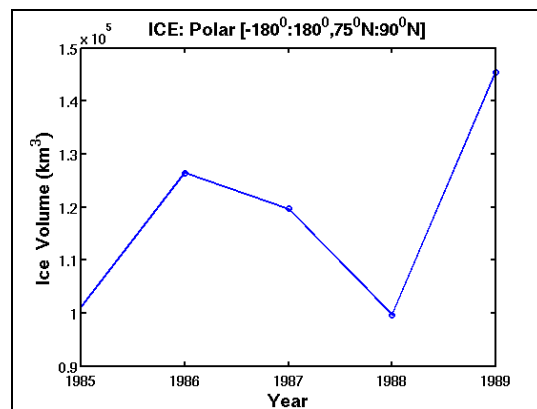
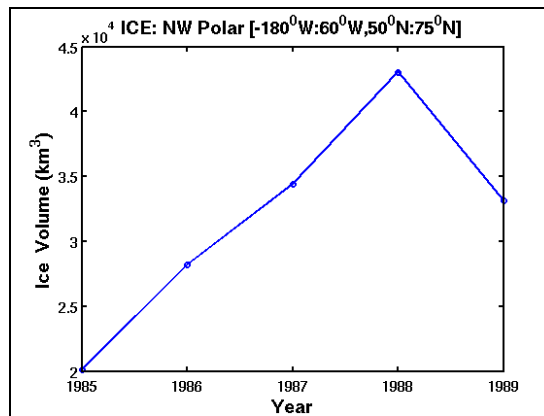
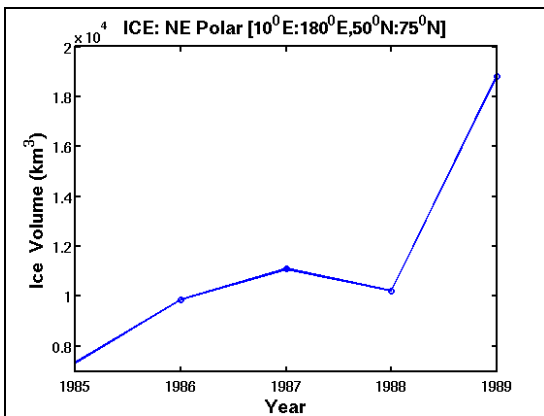
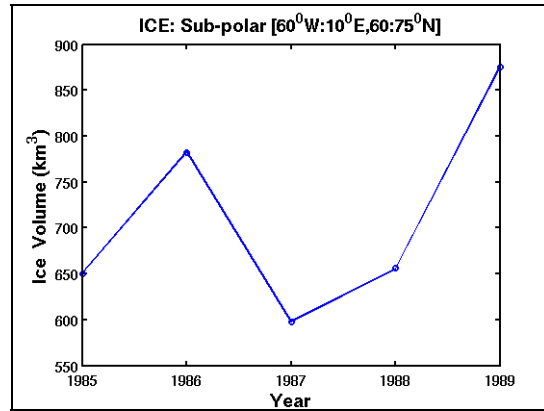
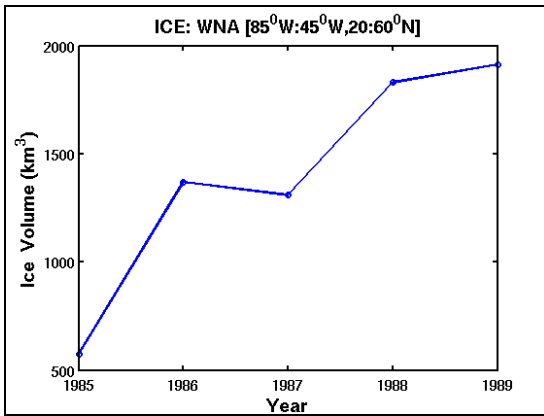


**Figure 9.** Ice trends in the 5 sub-domains.

## 2. Biogeochemical results and implementation plan

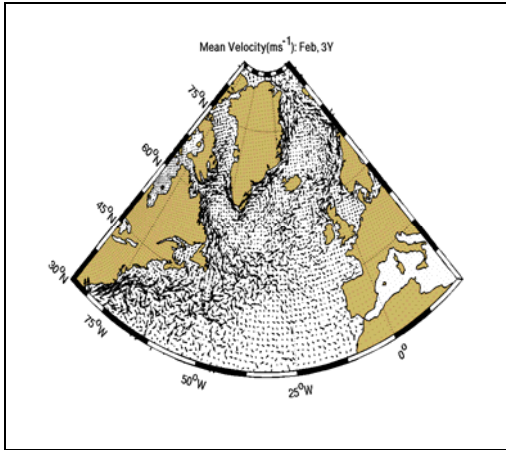
The mean modeled surface velocity averaged over three years of simulation was obtained for the months of February and March. The Slope Sea gyre is not pronounced during winter, but the Northern North Atlantic gyre and the Norwegian gyre are pronounced during these two months, as seen from Figure 10.

The mean modeled surface nitrate and silicate averaged over three years of simulation for February and March is seen in Figure 11. The model captures the winter deep mixing, which results in highest surface nutrients during March. The high surface nutrients in late winter set up the phytoplankton spring bloom in the North Atlantic. The model results also capture the higher surface nitrate than silicate concentrations, documented in a recent paper by Townsend et al. (2010). They also showed that this high N/Si ratio has decreased during the past five decades. In the future, we plan to use the lower resolution (LRW) ROMS-CoSiNE to simulate this decadal nutrient variability, and their influences on phytoplankton dynamics in the North Atlantic.

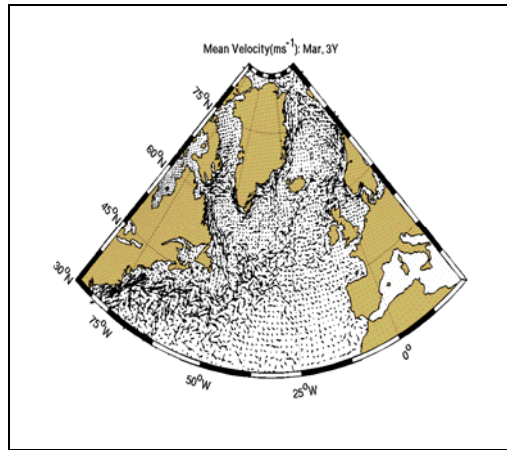
The modeled surface small phytoplankton and diatoms during May (A, B) and June (C, D) is seen in Figure 12. The modeled phytoplankton biomass is averaged over three year's simulation for May and June. The modeled diatoms tend to bloom first and progress towards higher latitude. The small phytoplankton bloom after the diatoms, then move to the north. Note that the biogeochemical model comparison presented in the 2009-2010 annual report showed clearly how the high-resolution model was an improvement in realizing the seasonal signals compared to the low resolution counterpart.

Figure 12 (A, C) clearly shows that the small phytoplankton first bloom in the WNA gyre and then the bloom is carried north with the NNA gyre. Figure 12 (B, D) shows that the diatom bloom in the NNA gyre is carried north with the Norwegian gyre.

The biogeochemical model results and figures clearly indicate that silicate and nitrate transport regulate diatom and small phytoplankton productivity respectively. The three gyres play an important role in the advection of the phytoplankton bloom northwards. The phytoplankton blooms occur in lower latitude in May, and then progress northwards in June. This is probably a consequence of incident light and mixed layer depth, as was shown by Siegel et al., 2002. Note that better HRW results in comparison to LRW gives us reasonable confidence in the biogeochemical parameterization and the same will be used with a "salinity corrected" physical model.

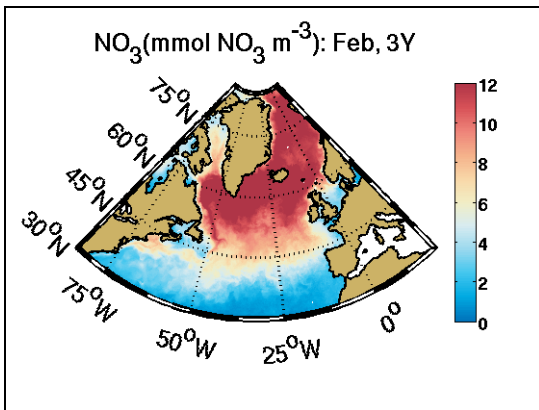


(A)

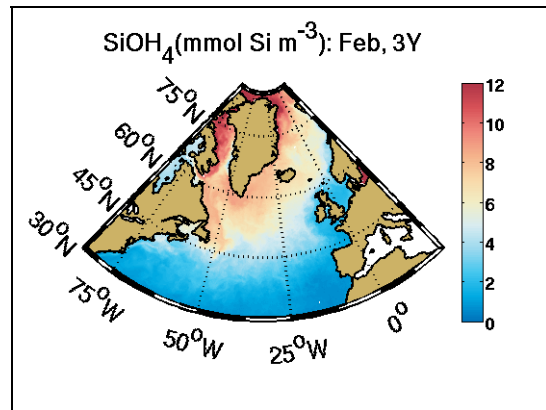


(B)

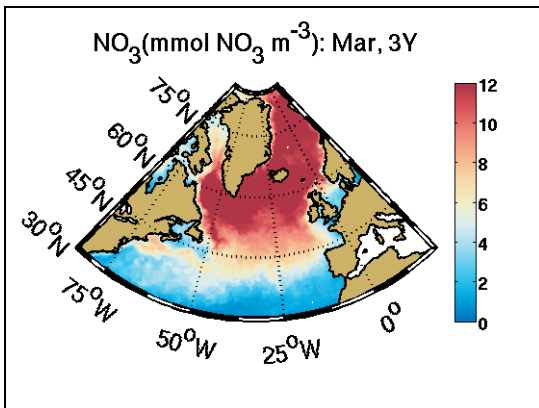
**Figure 10.** Mean modeled surface velocity for February and March.



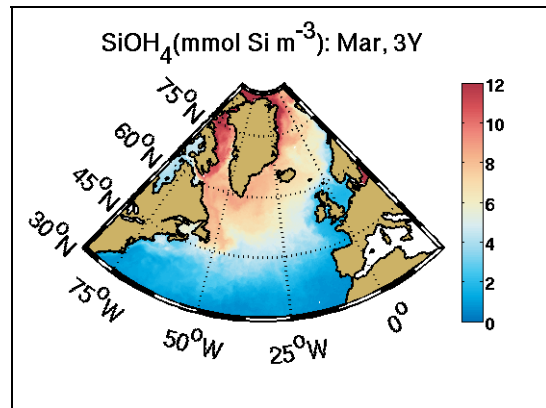
(A)



(B)



(C)



(D)

**Figure 11.** Modeled surface nitrate and silicate in February and March.

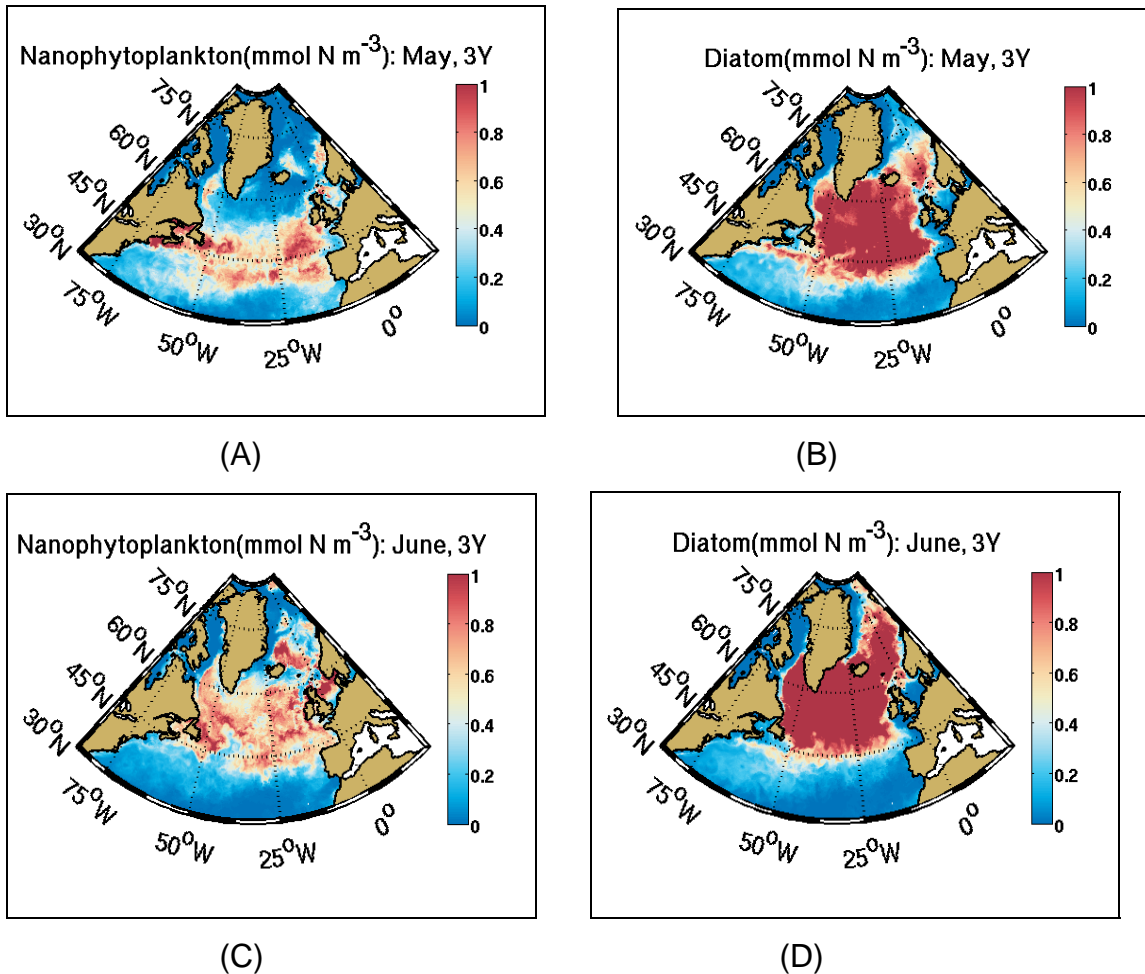


**Figure 12.** Modeled surface small phytoplankton and diatom in May and June.

### 3. *Climate Simulations Implementation Plan*

For the climate simulations, we are collaborating with Dr. Mike Alexander and Dr. Antonietta Capotondi of NOAA. After considerable group discussion in various PRS meetings over the last three years, we converged on the plan of forcing ROMS with difference fields (21<sup>st</sup> century minus 20<sup>th</sup> century) from the IPCC models. This type of experiment aims at understanding the regional-scale aspects of the large-scale changes in mean conditions. The use of difference fields is intended to minimize the influence of the known climate model biases in mean conditions. We will focus on the NCAR-CCSM3, and consider the SRES-A2 high-forcing scenario, which seems to better track the observed CO<sub>2</sub> evolution over the first ten years of the 21st Century. The differences will be computed between the second half of the 21<sup>st</sup> century and the second half of the 20<sup>th</sup> century (2050-2099 minus 1950-1999). The length of this simulation will be 20 years.

The following difference fields have been graciously prepared by Dr. Capotondi at the present time: (i) surface air temperature, (ii) surface air humidity, (iii) surface wind stresses; (iv) wind speed, (v) precipitation, (vi) radiation, and (vii) temperature T and salinity S over the whole 3D domain. The sensible and latent heat fluxes will be computed using the model SST and wind speed, air temperature and humidity. The T and S fields will be used for open boundary conditions as well as to initialize the T and S structure of the interior ocean to minimize spin-up time. The difference fields were first provided on the climate model grid and then interpolated on the ROMS grid. These fields are now ready for the proposed climate simulations which will be conducted after the model is configured to reduce the salinity drift.

#### 4. Summary and future tasks

The salinity drift seen in the model run in the first five years of the whole domain is primarily localized in the NW Polar, Sub Polar, NE Polar and Polar Regions, where systematic changes in salinity are observed. The results from the depth-binned salinity study of all the nine sub-domains further establishes that the salinity drift takes place in the upper 1000 – 1500 m of the ocean.

The future plans to reduce the salinity drift include: (i) modification of the ice initial conditions from climatology to January 1985, (ii) provision of open boundary conditions for the Bering Strait, (iii) improvement of the vertical mixing parameterization (implement KPP instead of GLS), and (iv) inclusion of inter-annual river run-off data in the model to account for the freshwater input into the model.

Based on the results obtained so far in the two 2-year long biophysical simulations, we are encouraged to continue running the biophysical simulations for the remaining period in the 1990's, i.e., 1992-1999. These runs will be carried out with the modified configuration (with correction for the salinity drift) and after implementing the monthly river runoff data from Dai and Trenberth (2002) and Dai et al. (2009).

A diagnostic method has been constructed among the collaborators (Haidvogel, Gangopadhyay and Chaudhuri) to quantify the effects of the primary factors responsible for the simulated salinity drift. These are E-P, River runoff (RR) and other freshwater input (*e.g.*, the Bering Strait), ice gain/loss, and possibly the freshwater flow through the Canadian Arctic Archipelago. First, we have quantified the salinity drift in each of the four regions: Arctic, Sub-polar, Sub-tropical and WNA. This non-conservative annual salt gain/loss over the regional volume was converted to a rate of missing/addition of freshwater to the 'ambient' or 'reference' salt content of that volume (*i.e.*, climatological volume-averaged salt content from Levitus). This rate, or the dilution factor, which is a rate of freshwater input ( $\text{m}^3/\text{s}$  per year) was compared with the observed E-P, RR, ice gain/loss and/or CAA through-flow as appropriate. Preliminary investigation points to a combination of E-P, RR and ice gain/loss in the polar regions.

In addition to the above diagnostics, we have begun implementing the monthly-varying river runoff input from the recently published Dai et al (2009) data set. This will replace the currently implemented annual mean precipitation representation of the RR which does not provide any seasonality. Finally, open-boundary implementations for the Bering Strait as well as the Mediterranean outflow are being devised based upon published values for transport and tracer properties (*e.g.*, Woodgate et al., 2005; Bryden et al., 1994).

In the fourth (current) year, our approach will be to quickly configure an LRW framework with (i) weak restoration of salinity (to compensate for E-P imbalances); (ii) inter-annual RR; (iii) KPP vertical mixing implementation; and (iv) January 1985 ice fields as initialization. We would like to run this LRW configuration for 10-15 years to evolve a dynamic-equilibrium state of the North Atlantic. We would use this LRW state to initialize the HRW set up and use the CORE2 forcing from 1985 to 2000 to develop the biophysical fields. This exploration with the LRW will be conducted in collaboration with our Rutgers colleagues, who are also exploring potential improvements to the LRW, as described next.

### **Low-resolution North Atlantic Workbench model (Rutgers)**

The low-resolution workbench (LRW) model has been implemented to satisfy three project goals:

- To provide an affordable modeling context within which to conduct the *Calanus* inverse modeling (see the next sub-section),
- To provide an efficient means of conducting many multi-year simulations for (*e.g.*) testing parameter variations and alternate forcing functions and boundary conditions, and
- To provide a platform with which to conduct an eventual 50-year retrospective simulation of physics plus ecosystems in the North Atlantic / Arctic basins.

#### *1. Initial design of the LRW, and prior results obtained (years 1 and 2)*

The low-resolution North Atlantic model has been configured based upon the Regional Ocean Modeling System

(<http://www.ocean-modeling.org/index.php?page=models&model=ROMS>).

The model grid covers all of the North Atlantic and Arctic Oceans and part of the South Atlantic up to 30° S. The grid has 192x284 horizontal grid points and 42 vertical layers. Resolution increases from 20 km in the western North Atlantic and the Arctic to 170 km in the Southern Atlantic. Plots of grid spacing and bathymetry are shown in Figure 13.

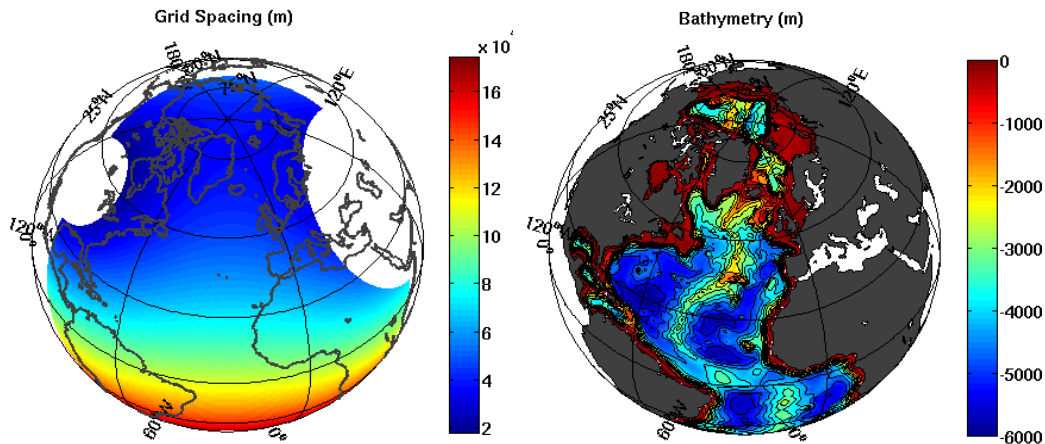


**Figure 13.** Model grid spacing (left panel) and model bathymetry (right panel)

The grid has had (until recently; see below) a closed boundary at the Bering Strait. At the southern boundary the model is forced by monthly climatological fields obtained from the 1958-2007 Simple Ocean Data Assimilation (SODA) re-analysis (Carton et al., 2000a, b) for velocity and sea surface height (SSH), and from the HYDROBASE climatology for temperature and salinity. Orlandi-type radiation open boundary conditions are used at the southern boundary.

To create initial conditions, the HYDROBASE climatology of the Atlantic Ocean was combined with the Levitus 2005 climatology for the Arctic Ocean. The new MOCHA climatology created at Rutgers University is used in the Middle Atlantic Bight (MAB). Velocity and SSH are from SODA climatological fields.

Air-sea heat and momentum fluxes are calculated by the bulk formulae of Fairall et al. (2003) using the corrected normal year analysis obtained from the 1958-2004 CORE model (Large and Yeager, 2004). The model has sea ice thermodynamics, but no tidal forcing. The combined HYDROBASE-LEVITUS-MOCHA monthly climatology is used for nudging temperature and salinity to avoid model drift from climatology. The time scale for tracer nudging is chosen large enough to allow proper geostrophic adjustment of the circulation fields. The time scale for temperature nudging is 20 days at the surface, increasing to 100 days at 1000 m depth; the time scale for salinity nudging increases from 50 days to 100 days from surface to 1000 m. The model time step is 0.25 hour.

The model has previously been spun up for nine years. Results of year 10 were used for validation. Climatology nudging ensures a good fit between the model and tracer climatology, as shown by TS profiles in Figure 14. For most of the profiles, the model agrees well with climatology. The worst agreement is observed in the regions that have sea ice (the EGC and LaS profiles) due to an overestimation of salt release by the ice model.

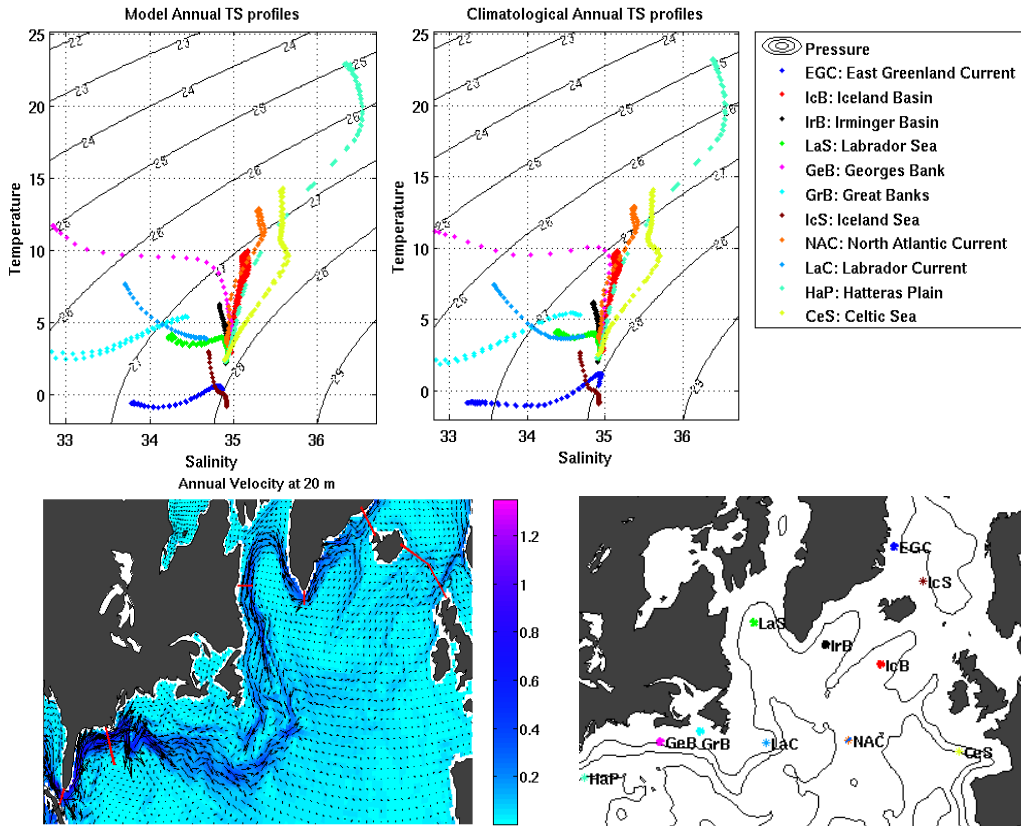


**Figure 14.** Top panel: comparison between the LRW ROMS model and climatological TS profiles at 11 different locations, identified in the lower right panel. Bottom left panel – annual velocity at 20 m depth.

Good agreement between the model and tracer climatology helps to ensure faithful representation of the main ocean currents in the model. The left plot of the bottom panel of Figure 14 shows annual mean velocity at 20 m depth. To evaluate the strength of the currents, we compute the transport through several key cross-sections (shown in red on the plot) and compare this with the estimates reported in the literature. This comparison is shown in Table 2. The model has correct transport through the Florida Strait. It also captures the exchange between the Nordic Seas and Northern North Atlantic reasonably well, although the return of the Nordic water through the Iceland-Scotland ridge is underestimated, with most of this water going to the North Atlantic through the Denmark Strait instead. The strength of the Gulf Stream and deep western boundary current is slightly under-estimated in the model. We believe that this is due to the lack of resolution in the Middle Atlantic Bight. In contrast, the Labrador Current is slightly stronger in the model than the observed values. Finally, it should be noted that these transport values were sensitive to the precise degree of topographic smoothing applied; considerable attention was devoted to the preparation of the bathymetry field.

	Model	Estimated
Denmark Strait inflow	0.6	1
Denmark Strait outflow	-8	-6
Iceland-Scotland inflow	6.9	7
Iceland-Scotland overflow	-0.5	-3
Transport at Cape Farewell (from shore to 2500m)	52	34-50
Labrador current (from shore to 2500m)	24	23 +/- 10
Gulf Stream at Cape Hatteras	59	70-90
Deep Western Boundary Current at Cape Hatteras	14	16-18
Transport at Florida Strait	30	31

**Table 2:** Annual average transport (in Sv) through several key sections: The second column is from ROMS; the third column are estimates from the literature (Hansen, Osterhus, 2000; Cuny et al, 2002; Han and Tang, 2001).

Figure 15 compares model mean sea surface height (SSH) with the mean dynamic topography (MDT) from AVISO. Apart from a slight overshooting of the Gulf Stream at Cape Hatteras, the main currents are represented well in the model. Especially good agreement is obtained in the sub-polar gyre, although its strength is slightly exaggerated in the model. The model also shows reasonable agreement with the MDT in the Nordic Seas. The worst agreement is in the MAB shelf area. This is a problematic area both for the model (lack of resolution) and for the data (contamination of the altimeter signal by the land).

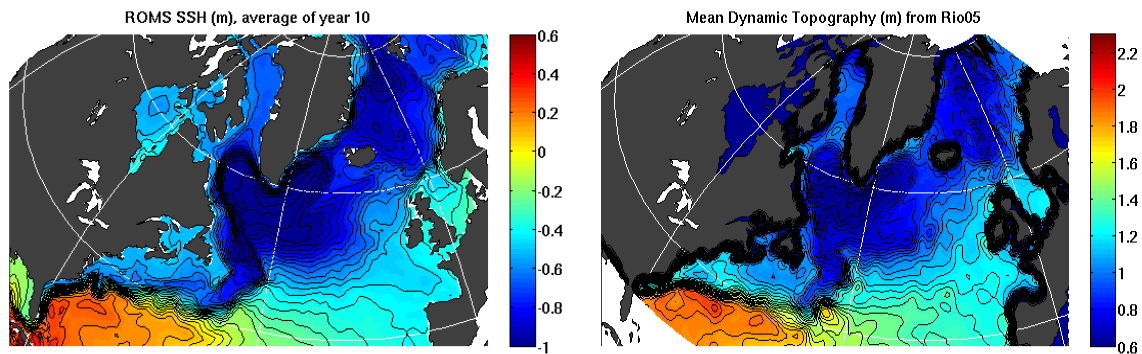


**Figure 15.** Left panel: mean SSH from ROMS, right panel: MDT from AVISO.

## 2. Findings in Year 3

Despite many features in respectable quantitative agreement with observations, several details of the initial LRW simulations were less creditable. In particular, our initial experience with the LRW (and the HRW) in Years 1 and 2 identified several key issues that needed further exploration and resolution. The most important of these include:

- the remaining departures from observed tracer climatology, in particular, the drifts in salinity in the polar and sub-polar regions;
- the accompanying (and presumably related) build-up of sea ice within some regions of the Arctic Basin;
- the anomalous freshening in the simulated Eastern North Atlantic; and
- the rapid (in some regions) loss of vertical stratification and tracer extrema at mid-depth.

In response to these concerns, in Year 3 we began to explore some variations in implementation that we hoped would (first) pinpoint the origin(s) of these limitations, and (second) reduce their impact.

The hypotheses underlying these sensitivity studies were:

- first, that the rapid salting of the polar and sub-polar regions was a consequence of the rapid (and erroneous) increase in sea ice volume, and that the latter was related to (a) the lack of exchange between the Arctic Ocean and the North Pacific via the Bering Strait and (b) limitations in the treatment of fresh water runoff;
- second, that the erroneous freshening of the Eastern North Atlantic was an obvious result of the lack of input of warm/salty water from the Mediterranean; and
- finally, that the rapid degradation of vertical stratification (and other anomalous features, such as the Gulf Stream over-shoot) was a consequence (perhaps inevitable) of the coarse horizontal resolution of the LRW.

In Year 3, we focused our attention on the first of these issues. To do so, the LRW was re-configured with the following modifications and enhancements:

- an inflow/outflow condition was added to represent water exchange at Bering Strait;
- a new treatment for river runoff was introduced;
- all restoration of salinity and temperature was removed except for a weak (360 time scale) relaxation to surface salinity;
- vertical resolution was increased to 50 terrain-following levels, and the newest algorithm for sigma coordinate stretching was employed;
- initial conditions were obtained from SODA, and the climatological atmospheric forcing employed thus far was replaced with inter-annual forcing beginning in 1958.
- the surface boundary layer treatment of Fairall et al. was replaced with the Common Ocean-Ice Reference Experiment (CORE) data [Large and Yeager, 2004].; and
- a full implementation of the tides was introduced.

It was hypothesized that the new features (in particular, the first three) would produce a stable sea ice pattern (distribution, volume, etc.) and minimize salinity drifts associated with anomalous salt rejection.

This first sensitivity study has been conducted thus far for a total elapsed time of 45 years. The resulting time series of sea ice volume is shown in Figure 16. The changes introduced to the LRW implementation do indeed produce a stable ice simulation in which the inter-annual variability is clearly visible. Note in particular the systematic reduction in sea ice volume in the contemporary period 1998-2003.

Additional sensitivity studies are underway to explore the addition of a source of Mediterranean water and the potential benefits of moderately increased horizontal resolution.

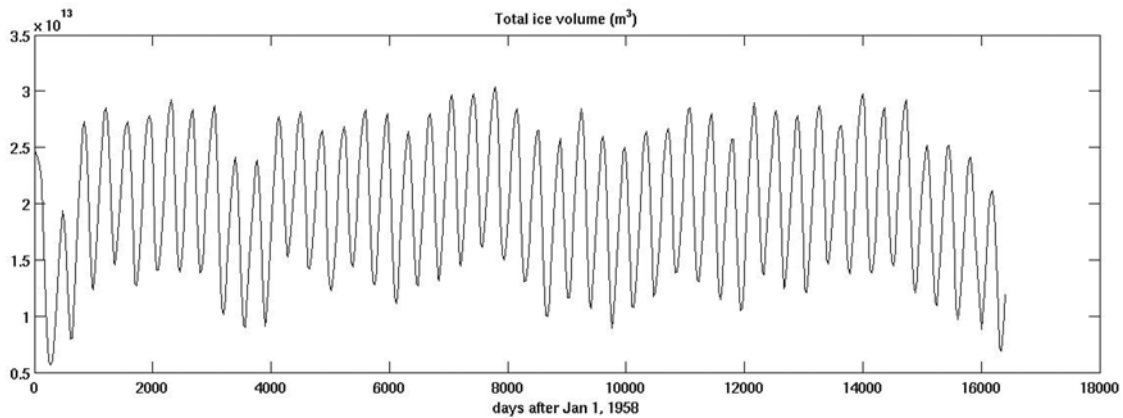


**Figure 16:** Simulated sea ice volume for the first 45 years of the revised LRW simulation.

### **Inversions for the “mean state” of *C. finmarchicus* populations in the North Atlantic (WHOI & Rutgers)**

Our overall objectives are to perform inversions of the “mean state” of *C. finmarchicus* populations in the North Atlantic, including examination of:

- Climatological mean seasonal forcing
- Diapause entry hypotheses: food, photoperiod
- Diapause exit hypotheses: development, photoperiod
- Control parameter: mortality (spatially variable, stage dependent)
- Skill assessment: cross-validation

We are further interested in investigating inter-annual to decadal variability in *Calanus* dynamics (e.g., high-NAO state vs. low-NAO states) and the eventual preparation of a 50-year hindcast (1950s-present) of the North Atlantic *Calanus* field.

In the last year, we have made significant progress on the overall objectives, as detailed next.

### 1. Physical model setup

The grid covers the North Atlantic, Arctic and South Atlantic down to 30°S. The grid has variable resolution, from 20 km in the western North Atlantic and the Arctic to 170 km in the South Atlantic. It has 280x190 grid points in the horizontal and 42 vertical levels. Time step is 1200 seconds. The model is initialized with Levitus 05 January climatology for temperature and salinity, and Simple Ocean Data Assimilation (SODA) reanalysis mean for velocity and sea surface height (SSH). Boundary conditions are from Levitus 05 monthly climatology for temperature and salinity, velocity and SSH are from SODA monthly mean. Surface fluxes are applied using bulk formulae. The model has sea ice, and rivers which are set as surface fresh water input. No tidal forcing is applied. The model is nudged toward climatology on a slow time scale. The model exhibits a climatological circulation pattern consistent with current understanding of the North Atlantic. In particular, the three gyres associated with the population centers of *C. finmarchicus* are resolved in the model.

### 2. *C. finmarchicus* observations

Monthly *C. finmarchicus* abundance is taken from the climatological CPR data set described in Beaugrand (2004). Units for abundance are number of individuals per 10 nautical miles of CPR record. The sample volume of 10 nm corresponds to approximately 3 m<sup>3</sup> according to Beaugrand. Sample depth is approximately 6.5 m.

### 3. Biological model setup

The problem is posed mathematically as an advection-diffusion-reaction equation for copepod concentration  $C$ :

$$\frac{\partial C}{\partial t} + v \cdot \nabla C - \nabla D \cdot \nabla C = R(x, y, z) \quad (1)$$

Velocity ( $v$ ) and diffusivity ( $D$ ) fields are specified from the hydrodynamic model described above. The biological reaction term  $R(x,y,z)$  is the simplest possible non-trivial formulation of sources and sinks that vary as a function of space only. Positive  $R$  can represent emergence from diapause and reproduction, whereas negative  $R$  can represent entry into diapause and mortality.

The CPR climatology provides estimates of near-surface concentration at monthly intervals  $t_i$  which we assume to be at the middle of each month:  $C_{obs}^{t_i}(x, y)$ . We interpret

these estimates as reflecting the concentration in the mixed layer, assuming uniform concentration between the surface and the mixed layer depth (MLD), defined to be the depth at which the modeled density rises  $0.05 \text{ kg m}^{-3}$  above the surface value (Figure 17, c.f. Figure 18). Below the mixed layer, we linearly interpolate between  $C_{obs}^i(x, y)$  and zero at a depth of twice the MLD.

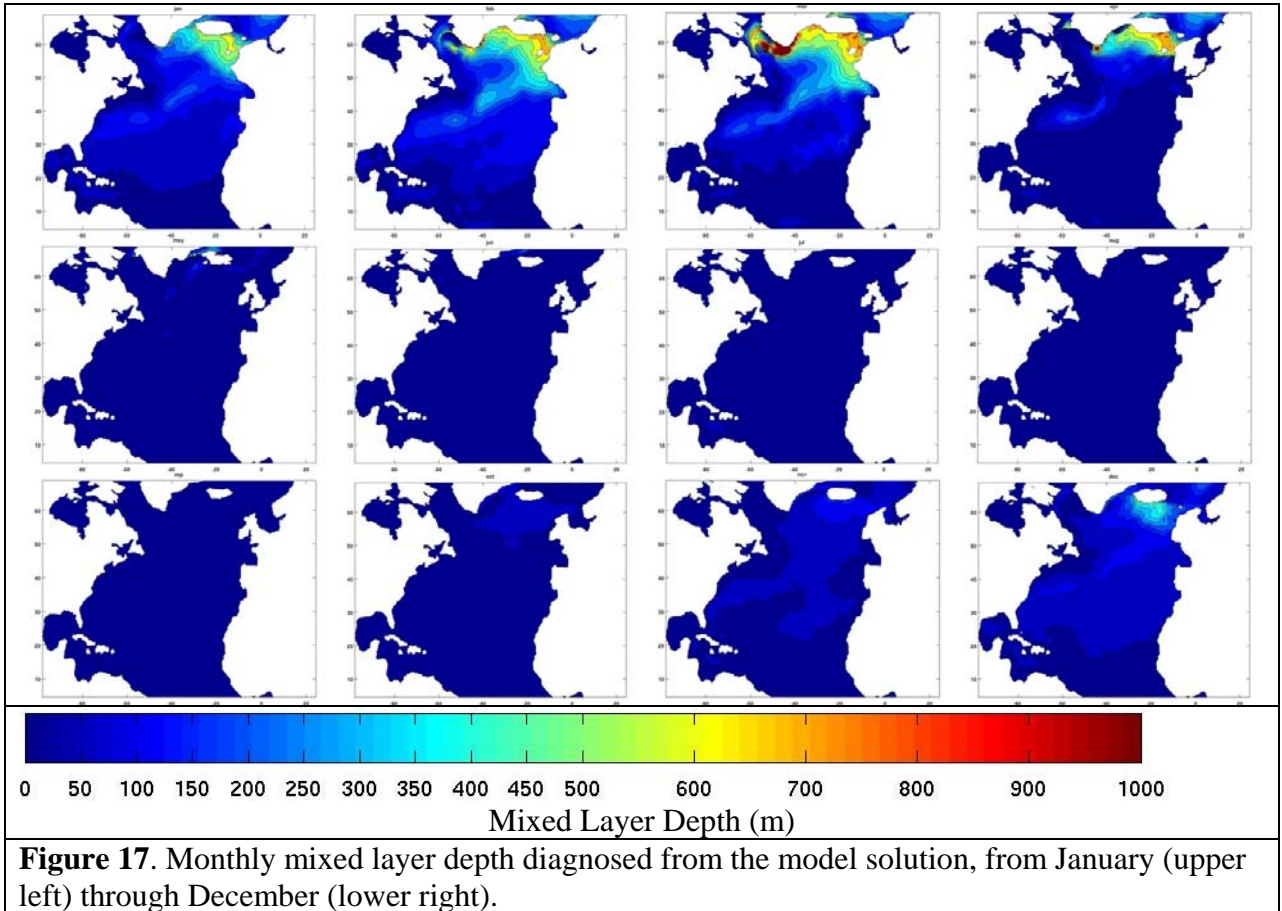


**Figure 17.** Monthly mixed layer depth diagnosed from the model solution, from January (upper left) through December (lower right).

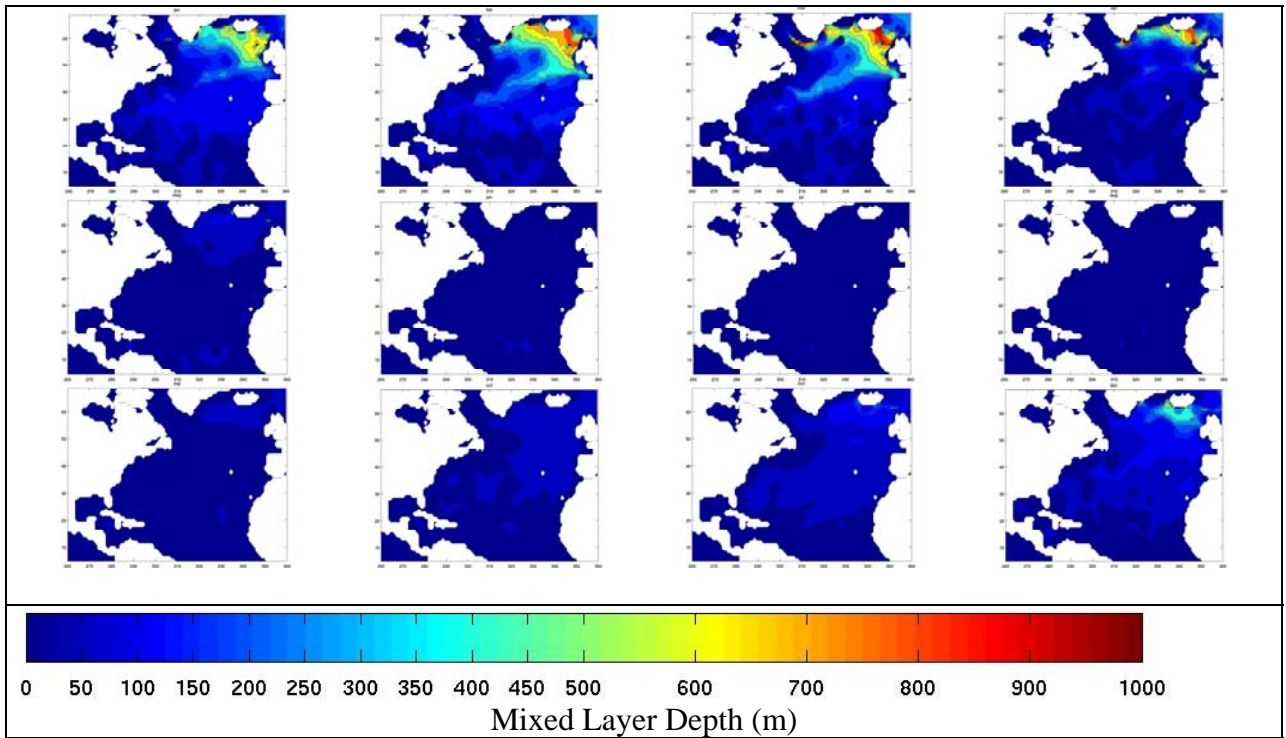


**Figure 18.** Monthly mixed layer depth diagnosed from the Levitus climatology, from January (upper left) through December (lower right).

The model is initialized with observations at time  $t_i$ , and we seek  $R_{t_i}(x, y, z)$  that will predict the concentrations observed the following month at time  $t_{i+1}$ . To find an optimal source term  $R_{t_i}$  we seek to minimize the cost function

$$J(R) = (HC_{t_{i+1}} - C_{t_{i+1}}^{obs})^T O^{-1} (HC_{t_{i+1}} - C_{t_{i+1}}^{obs}) + R_{t_i}^T B^{-1} R_{t_i}$$

where  $H$  is a measurement operator,  $O$  is the data error covariance, and  $B$  is the biological source term background error covariance. The solution is obtained by solving the following set of Euler-Lagrange equations:

$$\text{Forward model: } \begin{cases} \frac{\partial C}{\partial t} + v \cdot \nabla C - \nabla D \cdot \nabla C = R \\ \frac{\partial R}{\partial t} = 0, \quad t \in [t_i, t_{i+1}] \\ C(x, y, z, t_i) = C_{t_i} \\ R(x, y, z, t_i) = -B\mu(x, y, z, t_i) \end{cases}$$

$$\text{Adjoint model: } \begin{cases} -\frac{\partial \lambda}{\partial t} - v \cdot \nabla \lambda - \nabla D \cdot \nabla \lambda = 0 \\ \frac{\partial \mu}{\partial t} = -\lambda, \quad t \in [t_{i+1}, t_i] \\ \lambda(x, y, z, t_{i+1}) = -H^T O^{-1} (HC_{t_{i+1}} - C_{t_{i+1}}^{obs}) \\ \mu(x, y, z, t_{i+1}) = 0 \end{cases}$$

Our error hypothesis for the *C. finmarchicus* abundance data is uniform, chosen to be roughly 10% of the mean abundance, i.e.  $\sqrt{O} = 0.5 \text{ m}^{-3}$ .

The source term background standard deviation is set to be large in the mixed layer  $\sqrt{B} = 5 \text{ m}^{-3} \text{ d}^{-1}$ , and small below  $\sqrt{B} = 0.1 \text{ m}^{-3} \text{ d}^{-1}$ . These values are somewhat arbitrary, but are chosen to allow  $R$  to be essentially unrestricted in the mixed layer, and to prevent significant variations in  $R$  below the mixed layer.

The horizontal decorrelation scale for the background error covariance is set to 100 km, and vertical decorrelation scale is 20 m. Observations of *C. finmarchicus* are assumed to be uncorrelated.

#### 4. Results

There are several useful benchmarks with which to test the efficacy of the 4DVAR procedure. *Persistence* assumes that the concentration in a given month is the same as it was in the preceding month, thus providing a forecast  $C_{obs}^{t+1} = C_{obs}^t$ . *Passive advection* assumes that the right hand side of Equation (1) is zero, i.e.  $R(x,y,z)=0$ . The *Poor Man's Adjoint* estimates the right hand side ignoring the effects of advection:

$$R(x, y) = \frac{C_{obs}^{t+1} - C_{obs}^t}{\Delta t}$$

To evaluate the skill of the various models, we compute the RMS difference between the predicted and observed concentrations at the end of each simulated month (Figure 19). As expected, 4DVAR produces results with the lowest overall misfit.

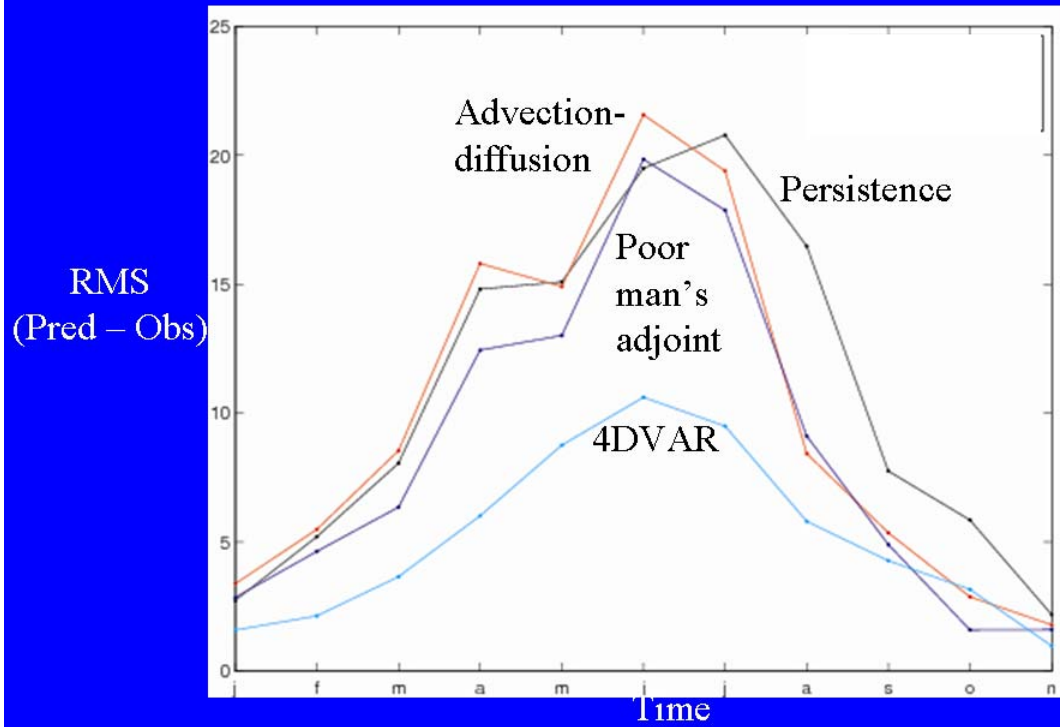
Predicted and observed *C. finmarchicus* fields for the 4DVAR inversions are depicted in Figures 20 (horizontal maps) and 21 (vertical sections). The latter illustrates a key assumption of these simplistic simulations, which is that the *C. finmarchicus* observations are assumed to represent the concentration throughout the mixed layer as diagnosed by the model. As such, MLD deepening causes dilution by entrainment of water with low concentrations of *C. finmarchicus*; likewise, MLD shoaling causes detrainment of *C. finmarchicus* below the mixed layer.

Term balances facilitate detailed diagnosis of the physical and biological factors regulating the seasonal variation of *C. finmarchicus* in the North Atlantic (Figure 22). Note that these vertically-integrated balances pertain to the entire water column and thus the source/sink terms do not show the same pattern of surface values of  $R(x,y,z)$  depicted in Figure 20. Indeed, there are significant vertical variations in  $R(x,y,z)$ , particularly during the springtime period of stratification and detrainment (April-May).

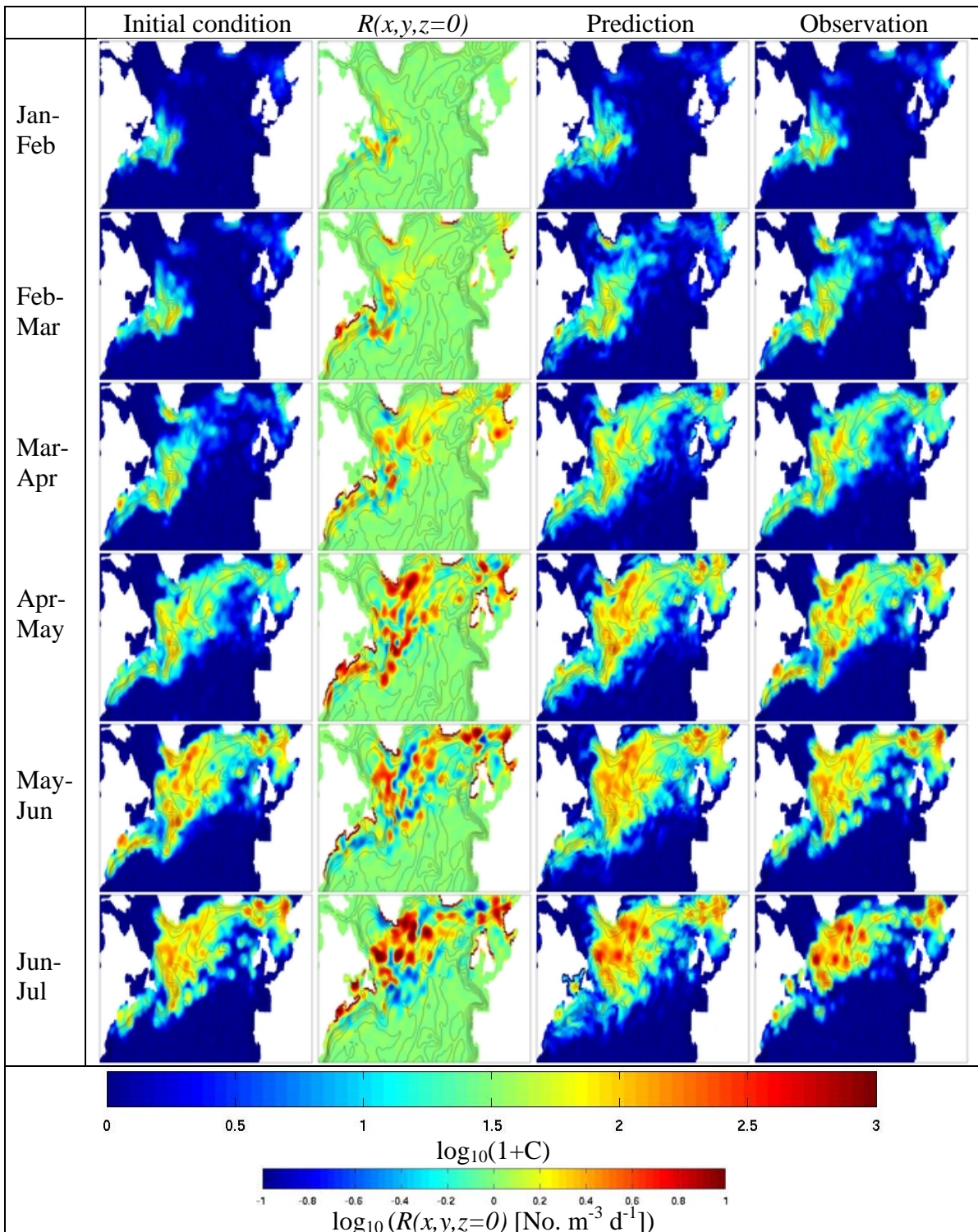
The model domain can be broken down into three distinct geographic regions corresponding to the three hypothesized population centers (Figure 23). Averaging the biological source/sink terms over each of the three sub-regions reveals significant seasonal variability, particularly in the central and eastern Atlantic (Figure 24, top). Hydrodynamic transport of *C. finmarchicus* between the regions also exhibits seasonal variation, and overall the transport terms are the same order of magnitude as the biological sources and sinks (Figure 24, middle). However, there are times when biological control far exceeds physical control, again in the central and eastern Atlantic population subdomains (Figure 24, bottom).

Clearly, the variations in physical and biological controls documented in Figure 24 are heavily impacted by the apparent mortality implied by detrainment of a large part of the population during springtime stratification. We are currently investigating two avenues: (1) analogous diagnostics couched in the upper layer only, and (2) reformulation of the inverse problem in a way that will reduce the sensitivity of the solution to the assumptions about vertical distribution of the organism.

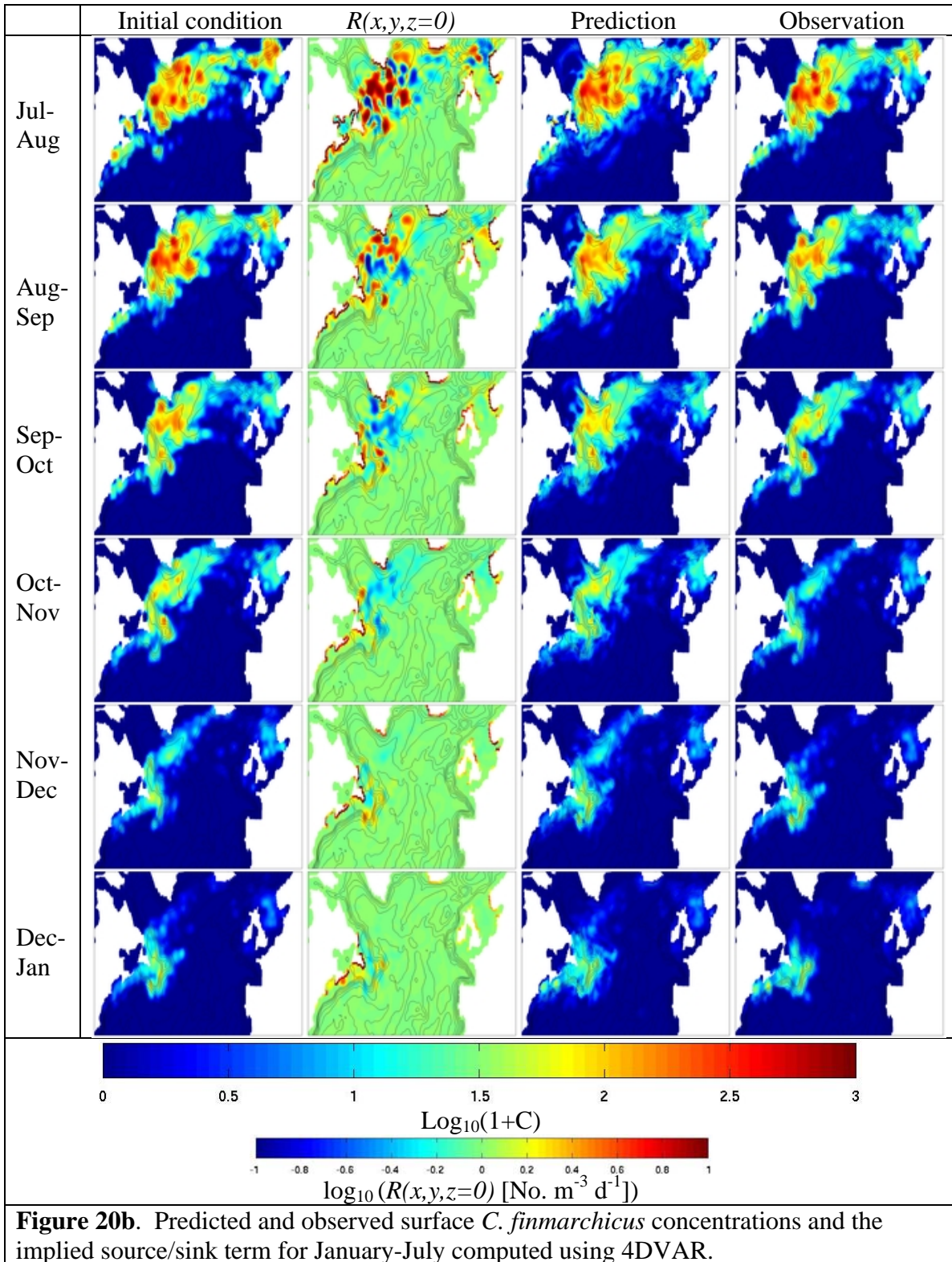
# Misfit



**Figure 19:** Time-series of misfit for four different models (see text): persistence, advection-diffusion, poor man's adjoint, and 4DVAR. Misfit is defined as the RMS difference between abundance at the end of each monthly simulation and the observed abundance for the following month.



**Figure 20a.** Predicted and observed surface *C. finmarchicus* concentrations and the implied source/sink term for January-July computed using 4DVAR.



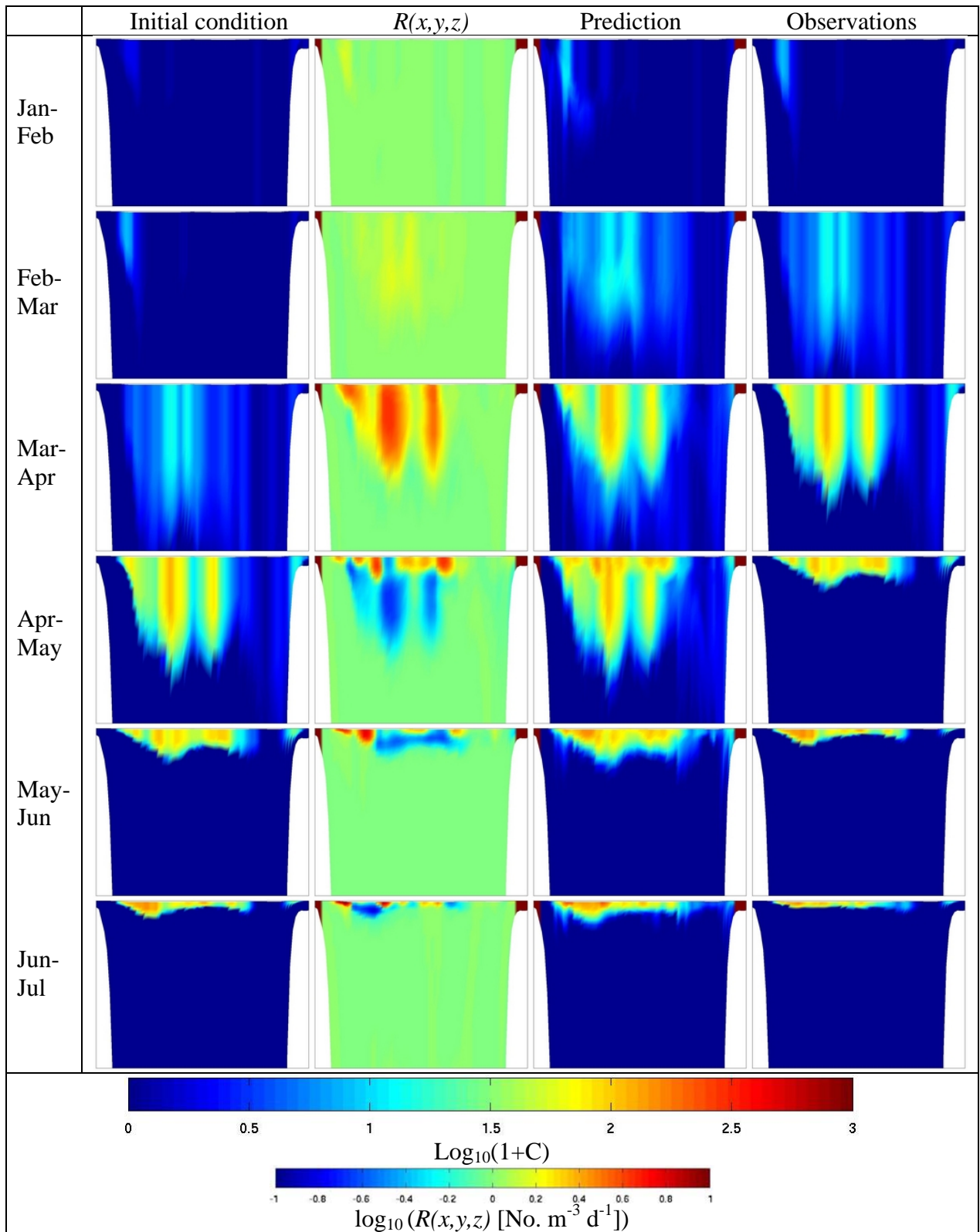


**Figure 21a.** Predicted and observed *C. finmarchicus* concentrations and implied source/sink term for January-July along a transect at 55N for the depth interval 0-1000m.

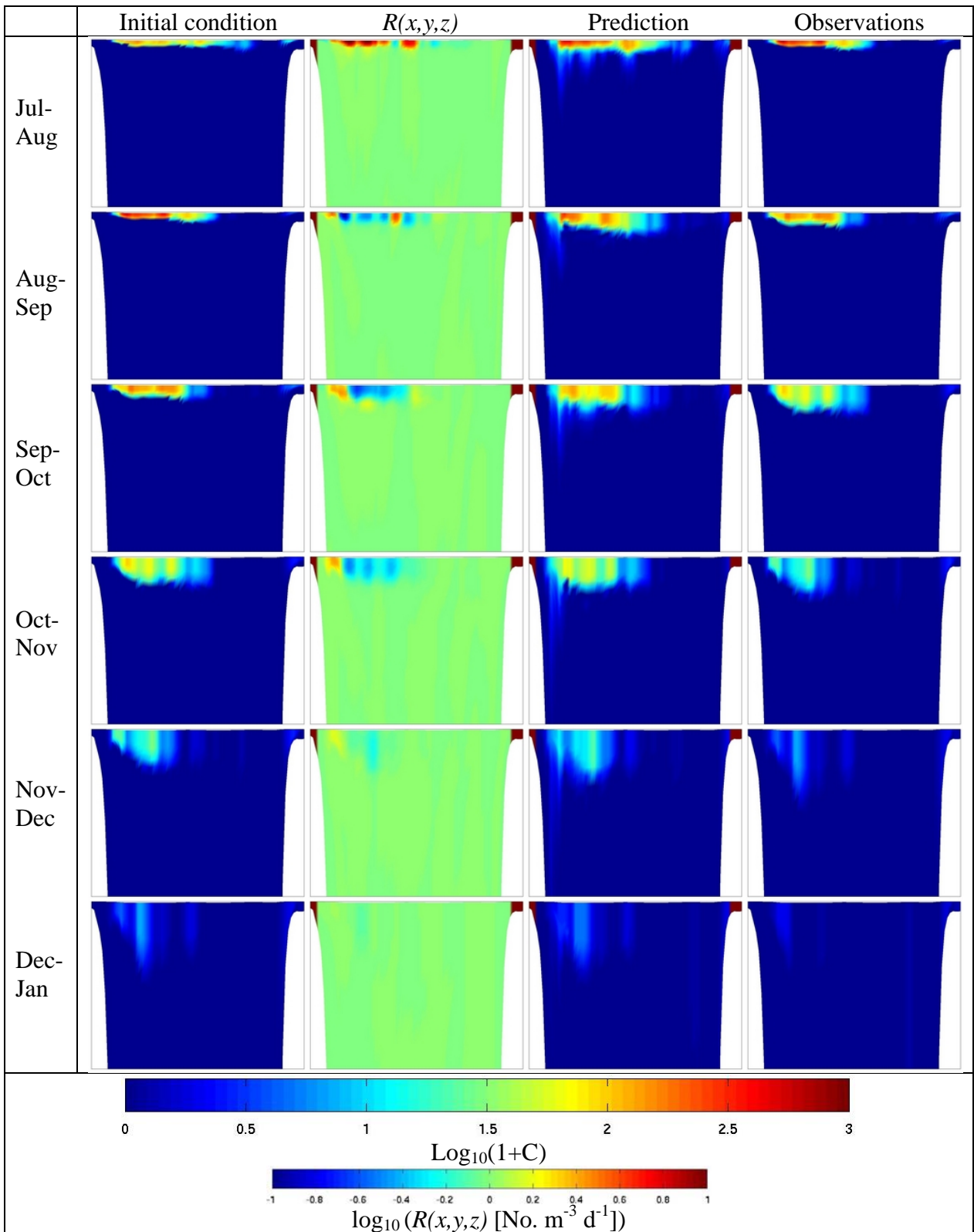


**Figure 21b.** Predicted and observed *C. finmarchicus* concentrations and implied source/sink term for July-January along a transect at 55N for the depth interval 0-1000m.

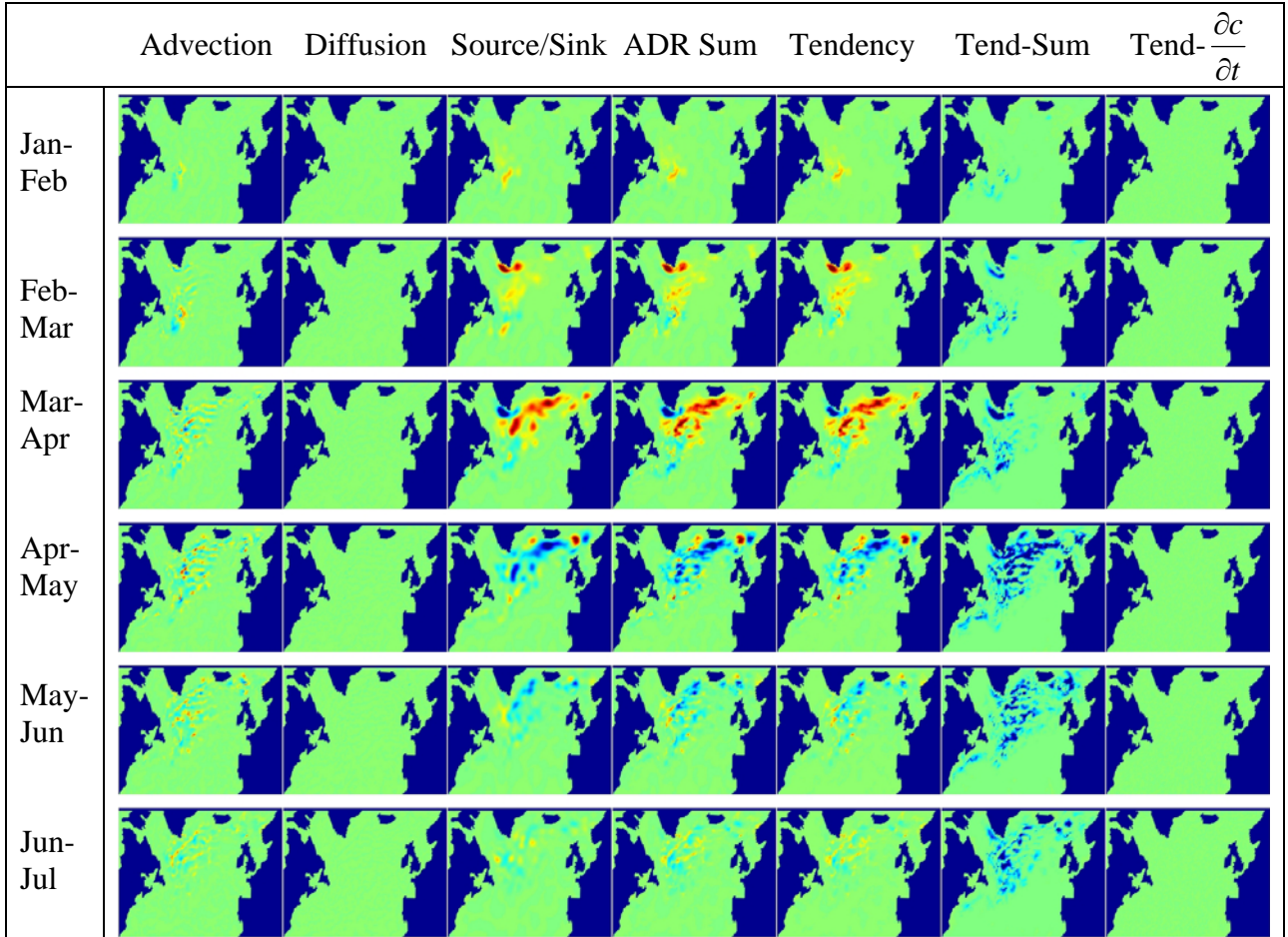


**Figure 22a.** Vertically-integrated term balances January-July: advection, diffusion, source/sink  $[R(x,y,z)]$ , ADR sum [advection plus diffusion plus  $R(x,y,z)$ ], tendency  $\frac{c_{i+1} - c_i}{t_{i+1} - t_i}$ , tendency minus ADR sum, and tendency minus the accumulator for  $\frac{\partial c}{\partial t}$ . The latter column demonstrates that  $\frac{c_{i+1} - c_i}{t_{i+1} - t_i}$  is a good approximation to  $\frac{\partial c}{\partial t}$ . The “Tend-Sum” column illustrates how the ADR sum is not the same as the tendency, by virtue of the positive definite constraint.

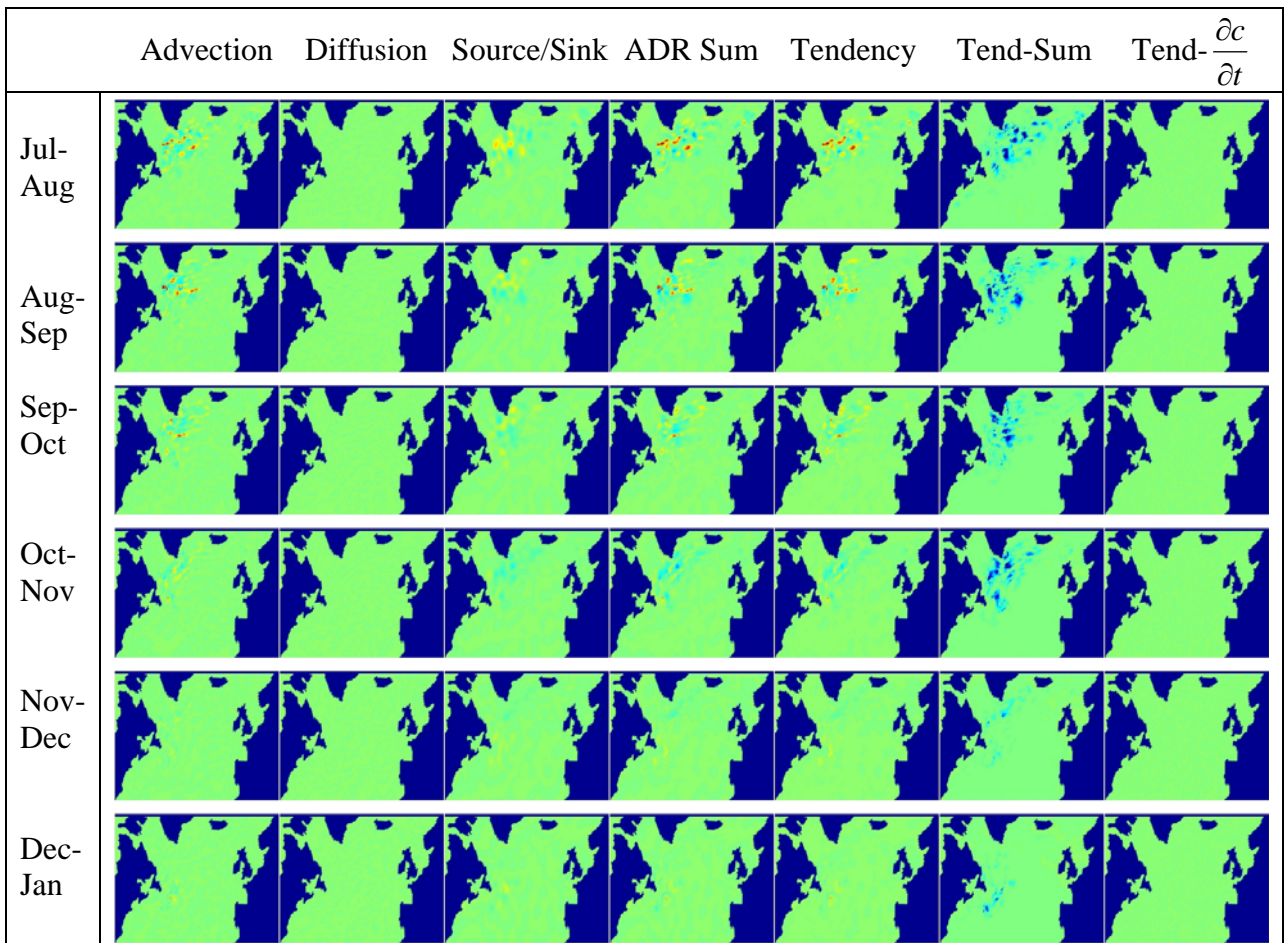


**Figure 22b.** Vertically-integrated term balances January-July: advection, diffusion, source/sink  $[R(x,y,z)]$ , ADR sum [advection plus diffusion plus  $R(x,y,z)$ ], tendency  $\frac{c_{i+1} - c_i}{t_{i+1} - t_i}$ , tendency minus ADR sum, and tendency minus the accumulator for  $\frac{\partial c}{\partial t}$ . The latter column demonstrates that  $\frac{c_{i+1} - c_i}{t_{i+1} - t_i}$  is a good approximation to  $\frac{\partial c}{\partial t}$ . The “Tend-Sum” column illustrates how the ADR sum is not the same as the tendency, by virtue of the positive definite constraint.

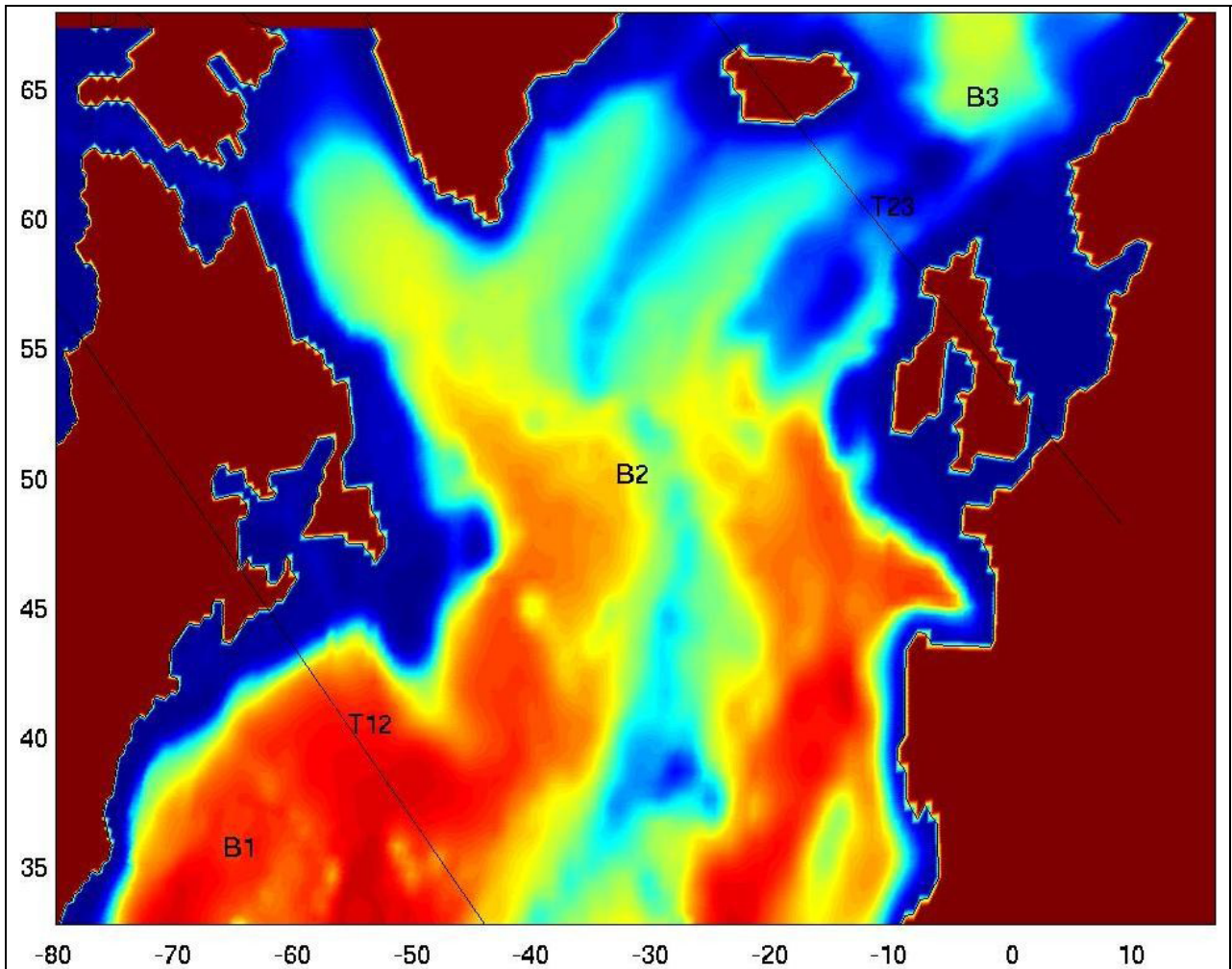


**Figure 23.** Breakdown of the model domain into the three geographic population centers: B1, B2, and B3. Transects T12 and T23 define the boundaries between them. Color shading represents bathymetry.

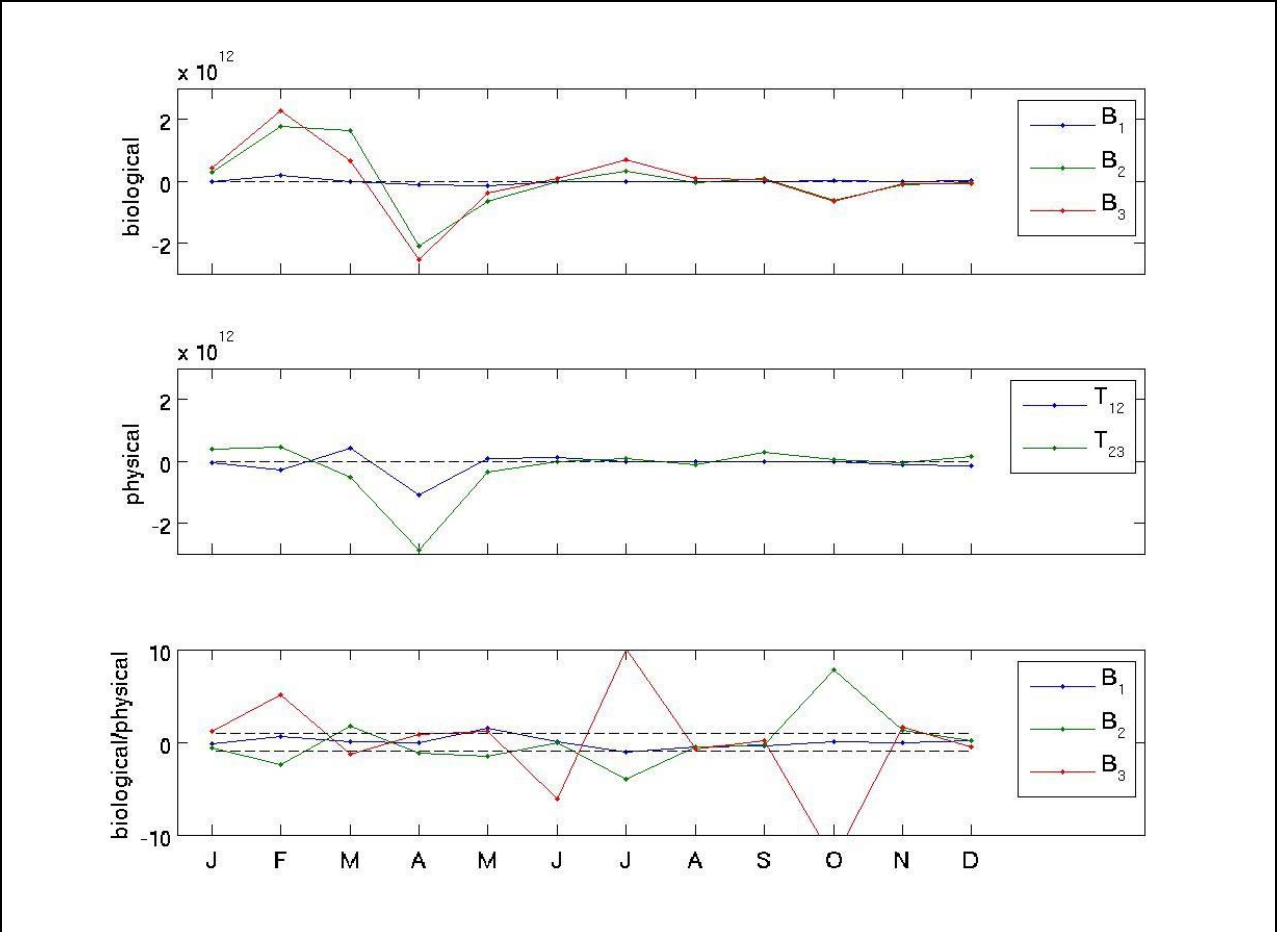


**Figure 24.** Time series of source/sink terms (top), fluxes across control surfaces T1 and T2 (middle), and ratio between biological and physical controls on the three population centers (bottom). Units of the upper two panels are  $\text{No. m}^{-3} \text{d}^{-1}$ , whereas the bottom panel is non-dimensional.

## Use of genetic data to estimate the rate of population exchange between gyres (UConn)

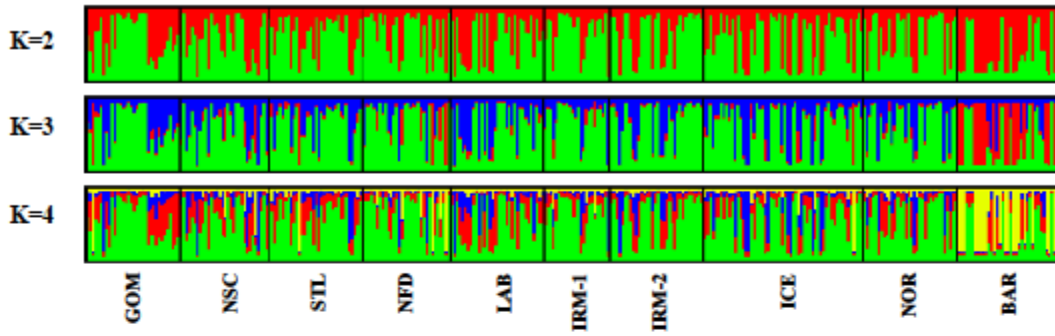
Population genetic analysis of *C. finmarchicus* examined allelic variation at 24 single nucleotide polymorphic (SNP) sites in three nuclear protein-coding genes: citrate synthase, heat-shock protein 70, and AMP-activated protein kinase. Samples were collected during 2005 from 10 areas representing the Northwest, North Central, and Northeast Atlantic gyres. Hypotheses of two or more distinct populations of *C. finmarchicus* were examined based on SNP variation within the three genes analyzed both separately and together using AMOVA (*Arlequin* Ver. 3.11), CLUMPP (Ver. 1.1), GENALEX (Ver. 6.2), *Genepop* (Ver. 4.0.10), and *Structure* (Ver. 2.3). All analyses revealed evidence of small but significant differentiation among areas within gyres (e.g.,  $F_{SC} = 0.0306$ ,  $p = 0.0000$  for two populations;  $F_{SC} = 0.0344$ ,  $p = 0.0000$  for three populations; pairwise  $F_{ST}$  values for all 10 areas ranged from 0.0000 to 0.2400), which may reflect ecologically-important, short-term (on the order of months) variation driven by geographic variation in life history traits.

Support for underlying large-scale differentiation, which may reflect persistent barriers to gene flow associated with entrainment in ocean gyres, was provided by various analyses, with numbers of distinct *C. finmarchicus* populations ranging from two to four (Figure 25). Analysis of molecular variation supported two populations, while clustering and population assignment supported two, three, or four populations. The Barents Sea sample was especially distinctive: one test using AMOVA was non-significant among gyres without this sample and differentiation among area populations within gyres was reduced. Analysis of additional genes, higher resolution sampling, and comparisons across different years are needed to resolve the spatial limits and number of distinct *C. finmarchicus* populations across the N. Atlantic Ocean basin.

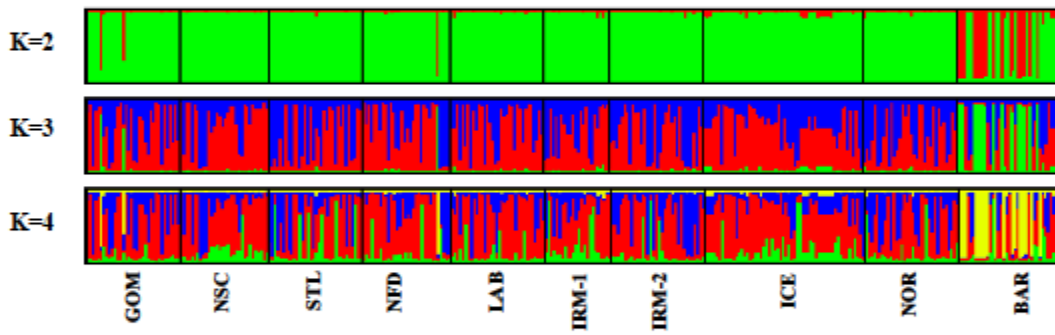
A manuscript on basin-scale population genetic structure of *C. finmarchicus* was published (Unal and Bucklin, 2010). In the course of sampling and analysis for this paper, spin-off studies by visiting UConn students revealed unexpected results for other copepod species (Aarbakke et al., 2011).

Figure 25

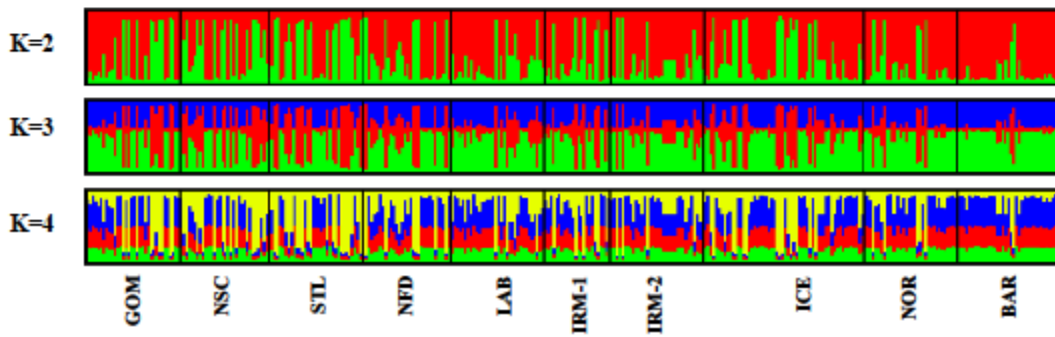
(a) AMPK gene



(b) CS gene



(c) HSP gene



## References

- Aarbakke, O.N.S., A. Bucklin, C. Halsband-Lenk, and M.F. Norrbin. 2011. Discovery of *Pseudocalanus moultoni* Frost 1989 in Northeast Atlantic waters based on mitochondrial COI sequence variation. *Journal of Plankton Research* [doi: 10.1093/plankt/fbr057]
- Bryden, H. L., J. Candela, T. H. Kinder, 1994: Exchange through the Strait of Gibraltar, *Progress In Oceanography*, **33**(3), 201-248.
- Carton, J.A., G. Chepurin, X. Cao, and B.S. Giese, 2000a: A Simple Ocean Data Assimilation analysis of the global upper ocean 1950-1995, Part 1: methodology, *J. Phys. Oceanogr.*, **30**, 294-309.
- Carton, J.A., G. Chepurin, and X. Cao, 2000b: A Simple Ocean Data Assimilation analysis of the global upper ocean 1950-1995 Part 2: results, *J. Phys. Oceanogr.*, **30**, 311-326.
- Cuny, J., Rhines, P.B., Niiler, P.P., Bacon, S., 2002: Labrador Sea Boundary Currents and the Fate of the Irminget Sea Water, *Journal of Physical Oceanography*, **32**, 627-647
- Dai, A., and K. E. Trenberth, 2002: Estimates of freshwater discharge from continents: Latitudinal and seasonal variations. *J. Hydrometeorol.*, **3**, 660-687.
- Dai, A., T. Qian, K. E. Trenberth, and J. D Milliman, 2009: Changes in continental freshwater discharge from 1948-2004. *J. Climate*, **22**, 2773-2791
- Fairall, C. W., E. F. Bradley, J. E. Hare, A. A. Grachev, and J. Edson., 2003. Bulk Parameterization of Air–Sea Fluxes: Updates and Verification for the COARE Algorithm, *Journal of Climate*, **16**, 571-591.
- Han, G., Tang, C.L., 2001: Interannual Variations of Volume Transport in the Western Labrador Sea Based on TOPEX/Poseidon and WOCE Data, *Journal of Physical Oceanography*, **31**, 199-211
- Hansen, B., Osterhus, S., 2000: North Atlantic – Nordic Seas exchanges, *Progress in Oceanography*, **45**, 109-208
- Large W. G. and S. G. Yeager, 2004: Diurnal to decadal global forcing for ocean and sea-ice models: The data sets and flux climatologies. *Technical Report TN-460+STR*, NCAR, 105pp.
- Planque, B., Hays, G.C., Ibanez, F. and Gamble, J.C., 1997. Large scale spatial variations in the seasonal abundance of *Calanus finmarchicus*. *Deep-Sea Research I*, **44**(2): 315-326.

Siegel, D. A., S. Maritorena, N. B. Nelson, D. A. Hansell, and M. Lorenzi-Kayser (2002), Global ocean distribution and dynamics of colored dissolved and detrital organic materials, *J. Geophys. Res.*, **107**(C12), 3228, doi:10.1029/2001JC000965.

Taylor, Karl E. (2001), Summarizing multiple aspects of model performance in a single diagram. *J. Geophys. Res.*, **110**, C11021, doi:10.1029/2005JC002902.

Townsend, D.A., Nathan D. Rebeck, Maura A. Thomas, Lee Karp-Boss, Rachel M. Gettings, 2010: A changing nutrient regime in the Gulf of Maine, *Continental Shelf Research* **30**, 820-832.

Unal, E. and A. Bucklin. 2010. Basin-scale population genetic structure of the planktonic copepod *Calanus finmarchicus* in the North Atlantic Ocean. *Progress in Oceanography* **87**: 175-186.

Woodgate, R. A., K. Aagaard, and T. Weingartner 2005: Monthly temperature, salinity, and transport variability of the Bering Strait throughflow, *Geophys. Res. Lett.*, **32**, L04601.